HIGH–RESOLUTION SEQUENCE STRATIGRAPHY AND XRF CHEMOSTRATIGRAPHY, OF THE AUSTIN CHALK

A Thesis

by

MARY ELIZABETH TRAPP

Submitted to the Graduate and Professional School of
Texas A&M University
in partial fulfillment of the requirements for the degree of

MASTER OF SCIENCE

Chair of Committee,	Arthur Donovan
Committee Members,	Michael Pope
	Stacey Lyle
Head of Department,	Julie Newman

December 2021

Major Subject: Geology

ABSTRACT

The Late Cretaceous Austin Group, across the outcrops and subsurface of Texas, are faced with numerous, often provincial, terminologies based on different lithologic, faunal, and petrophysical markers used to define internal units by various geoscientists. In order to define and map a more regionally consistent chronostratigraphic-based framework for the Austin Chalk across a four-county area in the southwest portion of the East Texas Basin, an integrated petrophysical, sequence stratigraphic, chronostratigraphic, and chemostratigraphic study was conducted. This study revealed that the Austin Group is an approximately 12-million-year (2^{nd}-order) unconformity-bounded depositional sequence, bounded by the K720sb at its base, and the K800sb at its top. A major internal unconformity, herein termed the K750sb was used to sub-divide the Austin Group into two, 3^{rd}-order, depositional sequences. This surface separates a carbonate-rich, unconformity-bounded, Lower Austin Formation below, from a more terrigenous-rich, unconformity-bounded Upper Austin Formation above. Within the Lower Austin Formation, a regionally mappable high gamma ray marker, interpreted as a maximum flooding surface, was used to define a Lower Member below from an Upper Member above. Each of these two members also have distinct petrophysical and chemostratigraphic characteristics. Similarly, within the Upper Austin Formation, another regionally mappable high gamma ray marker, also interpreted as a maximum flooding surface, was used to define a Lower Member below from and Upper Member above. Each of the two members within the Upper Austin Formation also have distinct petrophysical and chemostratigraphic characteristics.

Across the study area, the K800sb, which also defines the base of the overlying Taylor Group is a major erosional surface. This surface forms a north to south incision, commonly referred

to as the Waco Channel, which truncates into the Upper Austin Group across the study area. Interestingly, the thalweg of the Waco Channel, follows the present-day course of the Brazos River, suggesting a structural control to both. In terms of petroleum exploration, the primary target zone in the Austin Group is the lower member of the Lower Austin Formation, which is a carbonate-rich unit, distinctly devoid of clay rich partings, bounded by a bentonite bed. In general, this unit thickens from the northwest to the southeast of the study area, but only exceeds 40’ (13 m) in thickness in southeast Brazos County. Furthermore, a subunconformity play, targeting a potential carbonate-rich strata in the upper portions of the Upper Austin Formation, may also exist beneath the Waco Channel in the study area.

ACKNOWLEDGEMENTS

First and foremost, I would like to thank Apache Corporation for providing full funding, core access, data, and support on this project. I would also like to extend gratitude to Melissa Meyer for the encouragement to pursue higher education. I would also like to thank: 1) Brian Coffey and Stephanie Sosol, for your help and support describing cores and gathering core data; 2) Brent Miller for his chronostratigraphic work and TIMS age dates; and 3) Frank Sheppard and Mark Olson, for your help and support all throughout my graduate studies.

CONTRIBUTORS AND FUNDING SOURCES

This work was supervised by a thesis committee consisting of Dr. Arthur Donovan and Dr. Michael Pope of the Department of Geology and Geophysics and Dr. Stacey Lyle of the Department of Geography and the Zachry Department of Civil Engineering. Full funding for graduate study, core access, and data was provided by Apache Corporation. All other work conducted for the thesis was completed by the student independently.

TABLE OF CONTENTS

Page

LIST OF FIGURES

FIGURE PAGE

LIST OF TABLES

Table PAGE

1. INTRODUCTION

The Late Cretaceous Austin Group (Figure 1) is a fractured chalk play, whose play fairway parallels the U.S. Gulf Coast from Mexico to Florida across the subsurface (Figure 2). This play produces from numerous fields in Texas and Louisiana along a trend that extends over 300 miles (450 km) in length and over 40 miles (65 km) in width (Figure 2).

Since the 1920's, conventional drilling and completion techniques, with vertical wells, were marginally successful in developing fractured Austin Chalk reservoirs. However, in the early 1990's, the development of horizontal drilling techniques greatly enhanced the productivity of the wells by intersecting multiple fracture sets within the Austin Chalk, making it one of the first unconventional plays within the United States (Zuckerman, 2014). More recently, the combination of hydraulic fracturing and horizontal drilling, is used to unlock the Austin Group's unconventional resources.

The underlying Eagle Ford Group (Figure 1) is thought to be the primary source of most of the oil in the Austin Chalk, where hydrocarbons migrate upward through microfractures of the Eagle Ford Formation into the Austin Chalk filling the joints and charging its matrix porosity, with additional sourcing from the carbonate-rich beds within the chalk (Pearson, 2011). Historically, drilling operations targeted the heavily fractured zones within the Austin Formation, relying on the natural fractures to help facilitate hydrocarbon movement independent of a stimulus. However, as rapid reservoir depletion and decline rates in production have plagued previous drilling ventures, operators developed the combination horizontal borehole and multistage fracturing technique to help recover hydrocarbons trapped in the chalk's tight matrix porosity (Laurentian Research Group, 2019).

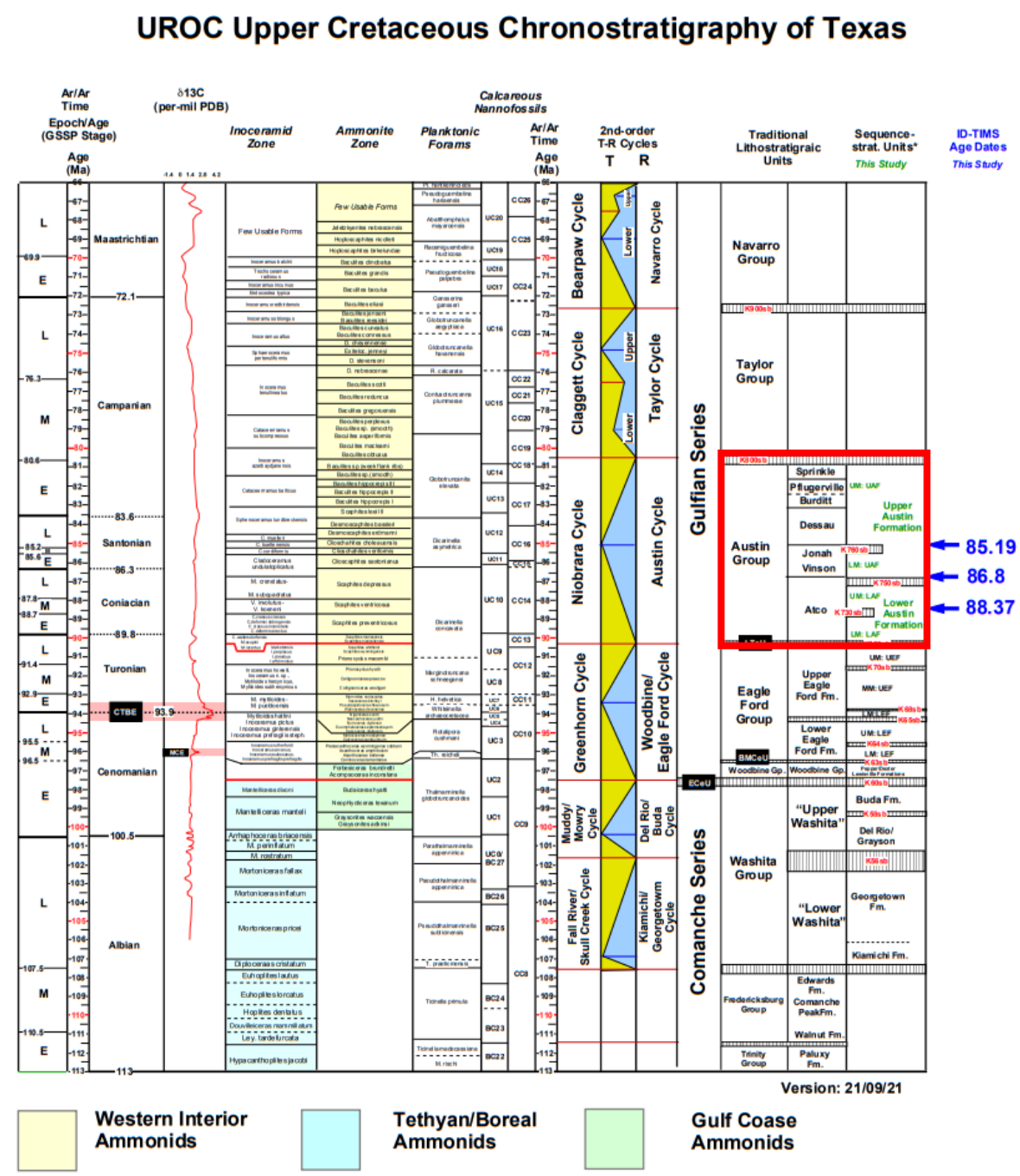

Figure 1. ICS Stages, macrofaunal zones, mega cycles, transgressive and regressive cycles, lithology, and δ13C global isotope profile for the Upper Cretaceous, courtesy of Art Donovan. Interval of study highlighted in red.

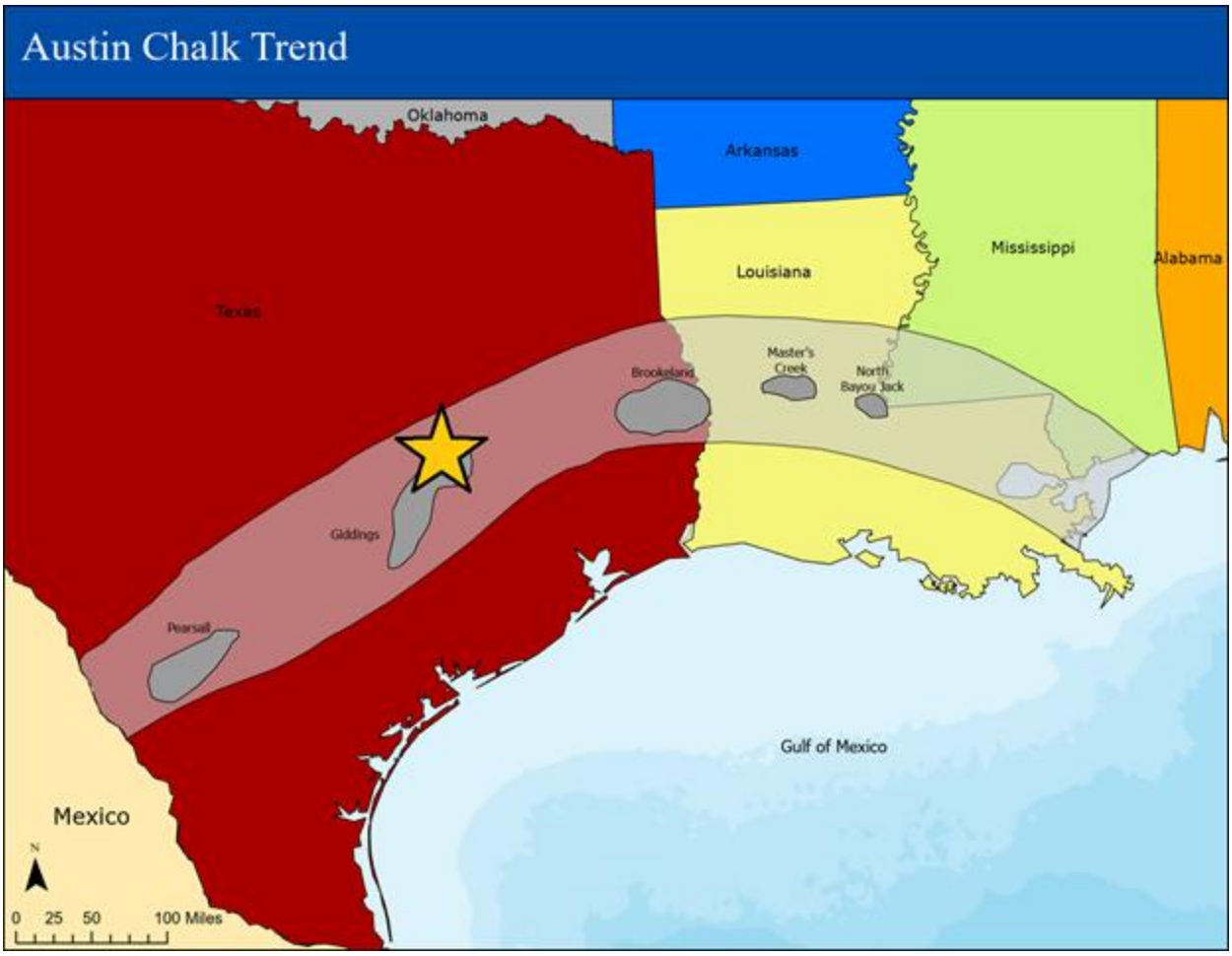

Figure 2. The classic Austin Chalk Play Fairway and associated major fields. Approximate study area location is starred (Parshall, 2017).

Within the Austin Chalk Play of Giddings Field in the southwest corner of the East Texas Basin (Figure 2), a grid of well-log cross sections, and an industry core referred to as Well-X, was studied to define an integrated sequence stratigraphic and chemostratigraphic framework for the Austin Group in this area. The goal, was that this framework would better explain and predict the vertical and lateral distribution of zones of high production within the Austin play fairway in this area.

1.1 Cretaceous Stratigraphic Overview

The Late Cretaceous earth (Figure 3) was a period of continental rifting, where the ancient continents moved toward their modern configuration, and large extents of shallow seas persisted globally. The Cretaceous period was a 'greenhouse world' where average surface temperatures were very warm due to high concentration of carbon dioxide in the atmosphere and higher average sea surface temperatures than today (O'Connor, 2019). Global sea level rose as a result of an expansion of the total volume of the mid-ocean ridges in combination with an increase in the rate of intrusion of the oceanic crust by plumes from the mantle throughout the Early Cretaceous with minor interruptions, resulting in widespread epicontinental seas and extensive marine deposits blanketing most continents (Stanley, 2015). Higher average water temperatures and high sea levels enabled coccoliths to proliferate in the shallow marine settings with respect to present-day North America depositing chalks on the seafloors (Figure 3). The Late Turonian through Early Campanian also coincides with the maximum extent of the Western Interior Seaway (WIS) where the Austin Chalk was deposited along its southern extent across the southern portion in present-day Texas, Louisiana, and Mississippi.

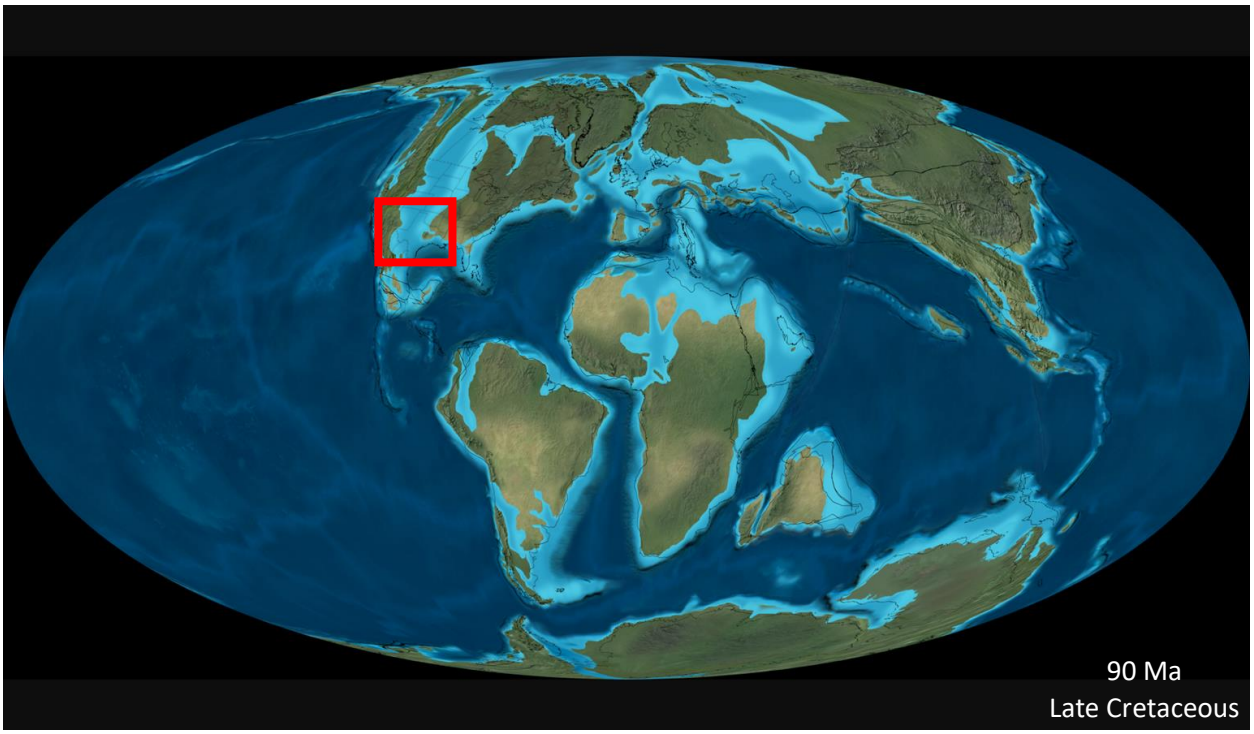

Figure 3. Global reconstruction of the Upper Cretaceous continental configuration approximately 90 Mya, during deposition of the Austin Group. The red highlighted box indicates the approximate location of the southern WIS (Blakey, 2019).

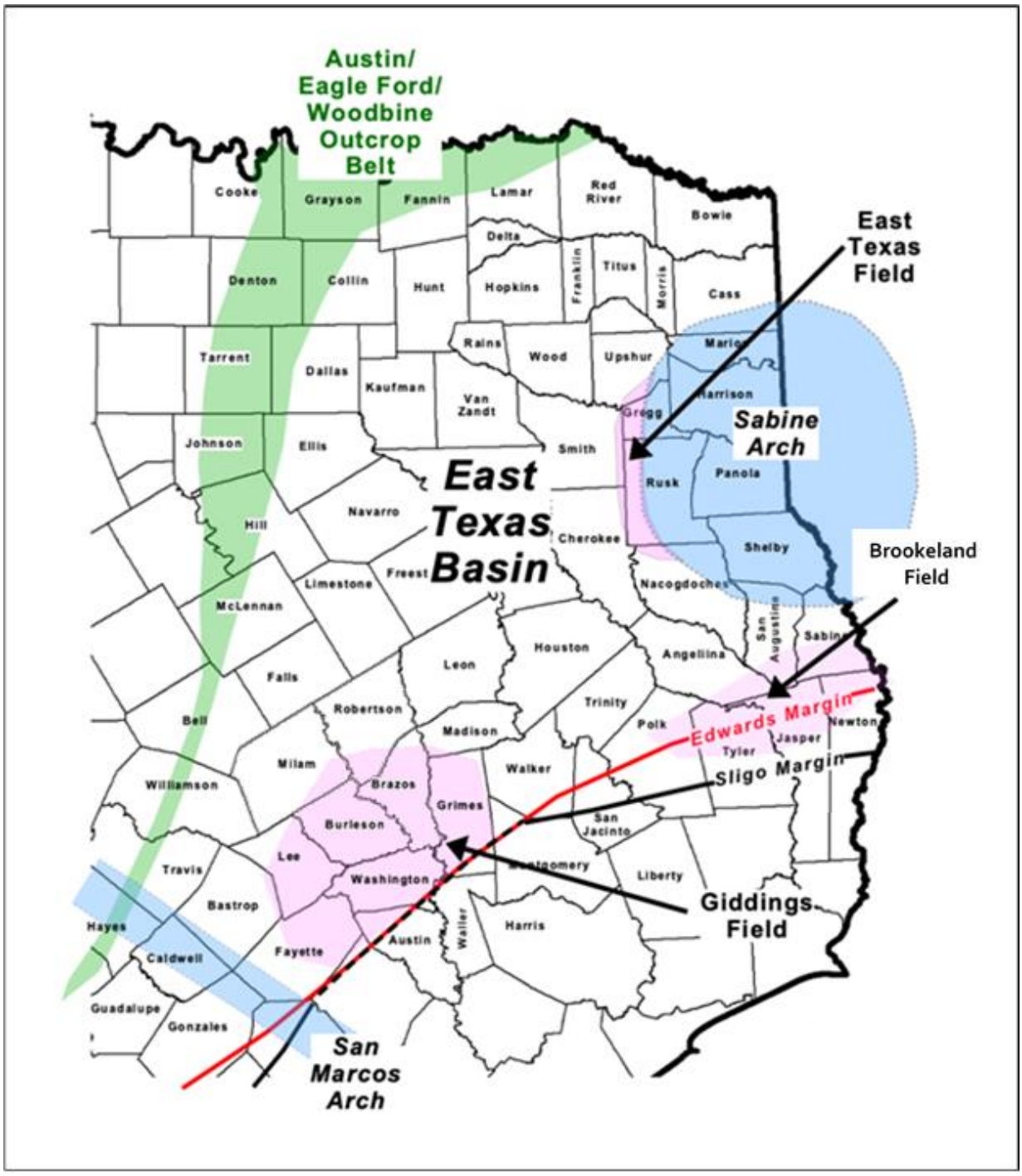

Figure 4. The classic Austin Chalk Play Fairway and associated major fields in the East Texas Basin (Donovan, 2019). This study is centered on four counties in Giddings Field.

1.2 Overview of the East Texas Basin

The East Texas Basin (Figure 4) is a Mesozoic paleo-physiographic feature defined by the Sabine Arch to the east, the San Marcos Arch to the southwest, the Cretaceous outcrop belt to the northwest, and the Lower Cretaceous Edwards Margin to the southeast. The East Texas Basin was once part of a more widespread Late Jurassic through Early Cretaceous continental shelf that was sub-divided by Latest Turonian foreland deformation, which uplifted the Sabine and San Marcos Arches (Jackson and Laubach, 1991). This Latest Turonian deformation also formed the East Texas Oil Field on the Western Flank of the Sabine Arch (Figure 4). This field is a sub-unconformity trap where fluvial-deltaic reservoirs of the Woodbine Group are regionally beveled and trapped by an angular unconformity at the base of the Austin Group (Halbouty, 1990). The Upper Cretaceous Austin Chalk is a low-permeability reservoir which produces oil and gas from major fractures oriented parallel to the underlying Lower Cretaceous Edwards Shelf Margin (Pearson, 2012). Horizontal drilling links these fracture systems to create an interconnected network, which drains the reservoir. The largest Austin Chalk Field in the East Texas Basin is Giddings Field.

1.3 Overview of the Austin Group

The lithostratigraphic term “Austin" was first used by Shumard in 1860 to define the Cretaceous limestone, which was used to build the State House, as well as several public buildings, in the capitol of Austin, Texas (Adkins, 1932). Over time this stratigraphic unit became more commonly known as the Austin Chalk. In his classic work on the Mesozoic stratigraphy of Texas, Adkins (1932) elevated the Austin Chalk to Group level, and he interpreted regional unconformities separating it from both the underlying Eagle Ford, as well as the overlying Taylor,

Groups. The Austin Chalk is a slightly burrowed, laminated marly chalk (wackestone) composed primarily of coccoliths (Loucks, 2021). This lithostratigraphic unit can be traced within the Middle Cretaceous outcrop belt across Texas (Person, 2012). Traditionally considered Coniacian to Early Campanian, with its lowermost portions now defined as Uppermost Turonian (Figure 2), the basal portions of the Austin Chalk change facies into the more sandstone prone Tokio and Eutaw Formations along the outcrop belt in Louisiana, Arkansas, and Mississippi (Clark, 1995).

Across what is now Texas, the Austin Chalk was primarily deposited in a shallow inner to middle shelf setting with paleowater depths that ranged from 30 ft, or less, to more than 300 ft (Dravis, 1979). Trace fossil assemblages, including *Planolites, Thallassinoides, and Chondrites,* indicate normal marine salinity with deposition in an open marine environment (Dawson and Reaser, 1990). Across the outcrop belt and subsurface of Texas, the Austin Chalk ranges in thickness from 150 to 800 ft (46 to 244 m; Pearson, 2012). In terms of the internal stratigraphy, the Austin Chalk was sub-divided into a portfolio of provincial surface and subsurface terms that are common in the literature (Figure 1). However, in a broader and more regionally applicable sense, Pearson's (2012) regional assessment of the Austin Group followed the framework suggested by Hovorka and Nance (1994), which sub-divided the Austin Chalk into three main units: 1) lower chalk, 2) middle marl, and 3) upper chalk (Figure 1). The upper and lower chalks contain less clay and are therefore better reservoirs because they are more brittle, leading to higher fracture density (Hovorka and Nance 1994). In terms of the internal lithology, an alternative sub-division of the Austin Chalk, commonly used in south Texas, is the Atco, Vinson/Jonah, Dessau, Burditt, and Pflugerville suggested by Young (1977). This naming convention divides the Austin Group based on lithology and faunal zones into regionally localized members.

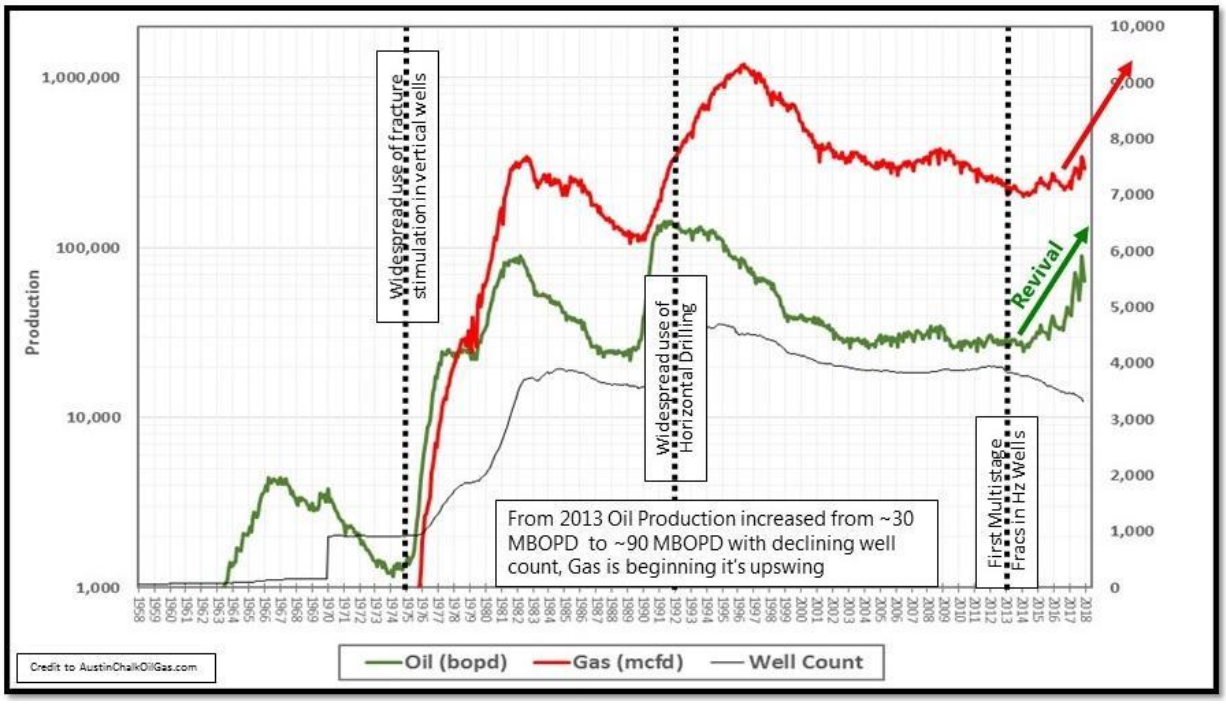

Figure 5. Historical production from the Austin Group, depicting timing of technological advances in hydrocarbon recovery, (Laurentian Research, 2019). Marked timings show approximate start of widespread fracture stimulation, horizontal drillings, and multistage fracs in horizontal wells.

1.4 Austin Chalk Historic Production & Play Challenges

As outlined on (Figure 5), the Austin Chalk's historical production is marked by the emergence of new technologies in hydrocarbon recovery. In the 1960's, vertical wells were drilled targeting the heavily fractured zones of the chalk (Laurentian Research Group, 2019). While initial production rates were promising, they quickly declined due to the rapid depletion of the open fracture system in the chalk. During the late 1970's, operators applied fracture stimulation techniques in the vertical wells to produce oil from within the tight matrix porosity, yet again resulting in a rapid increase in production. In the early 1990's, horizontal drilling was introduced within the Austin Chalk, extending the total wellbore length in the exposed pay zone. Beginning in 2013, the first combination multistage fracture in a horizontal well was used in the Austin Chalk helping wells produce more consistently, starting a revival in production. Oil production in the chalk subsequently increased that year from ~30 MBOPD to ~90 MBOPD despite a declining well count (Laurentian Research, 2019).

The Austin Chalk is a complex play consisting of conventional fractured carbonate reservoirs being enhanced and connected by modern drilling and completion techniques. Current play challenges for the Austin Chalk are the rapid decline and repeatability of well results and the challenges associated with optimizing a technique that will produce the chalk at consistent rates with a slow decline in a horizontal multistage frac well (Laurentian Research Group, 2019). Conversely, the proximity of the Austin Group to the Gulf Coast gives the formation a distinct advantage over other older plays; as adequate existing midstream infrastructure helps lower capital expenditure. Current breakeven prices for oil produced from the Austin Chalk is estimated to be ~$40 per barrel (Hagerty, 2018).

2. OBJECTIVES

The purpose of this study is three-fold. Firstly, to assess both models of the Bruker handheld XRF devices used in this study to determine which model most accurately represents the carbonate-rich Austin Chalk. Secondly, to create an integrated petrophysical, chemostratigraphic, chronostratigraphic, and sequence stratigraphic framework to define the internal markers within the Austin Group and correlate across the identified study area. And lastly, to identify, explain, and predict the distribution and thickness variations of key Austin zones.

The Austin Group's outcrops and cores tend to be fairly homogenous making it difficult to distinguish its internal members based on appearance alone. Thus, an integrated framework was created to define the Austin Group's members. Historically, very little research has been conducted on the Austin Group within the study area, and the previously mentioned naming patterns of Young (1977) and Hovorka and Nance (1994) only account for a small aspect of the Austin Group's varied stratigraphy leading to numerous terminologies relevant only to specific localities. Using the approach outlined in this study, the Austin Group's members can be identified regionally based on a more comprehensive naming convention which accounts for time of deposition, lithology, and depositional setting. This will prove beneficial for improving energy resources, as more accurately defined members will help identify and predict thickness variation for key productive zones.

3. METHODS

3.1 Study Area

This study spans four counties in southwest Texas near Giddings Field (Figure 6). Please note the actual county outlines were omitted as part of the data release. This study examines the Austin Group within a framework of well log cross sections, including 141 well logs and one core (Figure 6). Log data was sourced from Drilling Info, MJ Logs, and the Texas Water Development Board, exported as .las files and bitmap images. X-ray Fluorescence data was collected from the single industry core in Brazos County, Texas, Well-X. Fourteen cross sections were created and correlated across the study area using Petrel 2019.

3.2 High-Resolution XRF Acquisition

High-resolution X-ray fluorescence (XRF) data was collected using two models of the Bruker handheld spectrometer, the Bruker Tracer 5g and Bruker Tracer 5i, to compare and evaluate both records of elemental concentrations of the cored section and determine which model most accurately reflects the Austin Group. The handheld units gathered data over a collective span of 30 days, during which time, the core samples were in temperature-controlled environments and enclosed in their marked storage boxes, in order to maintain stable conditions between both runs of the handheld devices, preserving data integrity. XRF readings were taken on the core every 2.4” (6 cm) and compared to determine the best data set for the carbonate-rich Austin Chalk. Data was collected below log scale, 6” (15.2 cm), to capture the finer laminations and structures that would have otherwise been lost with coarser data resolution, ensuring all aspects of the core were reflected in the collected data instead of an average reading.

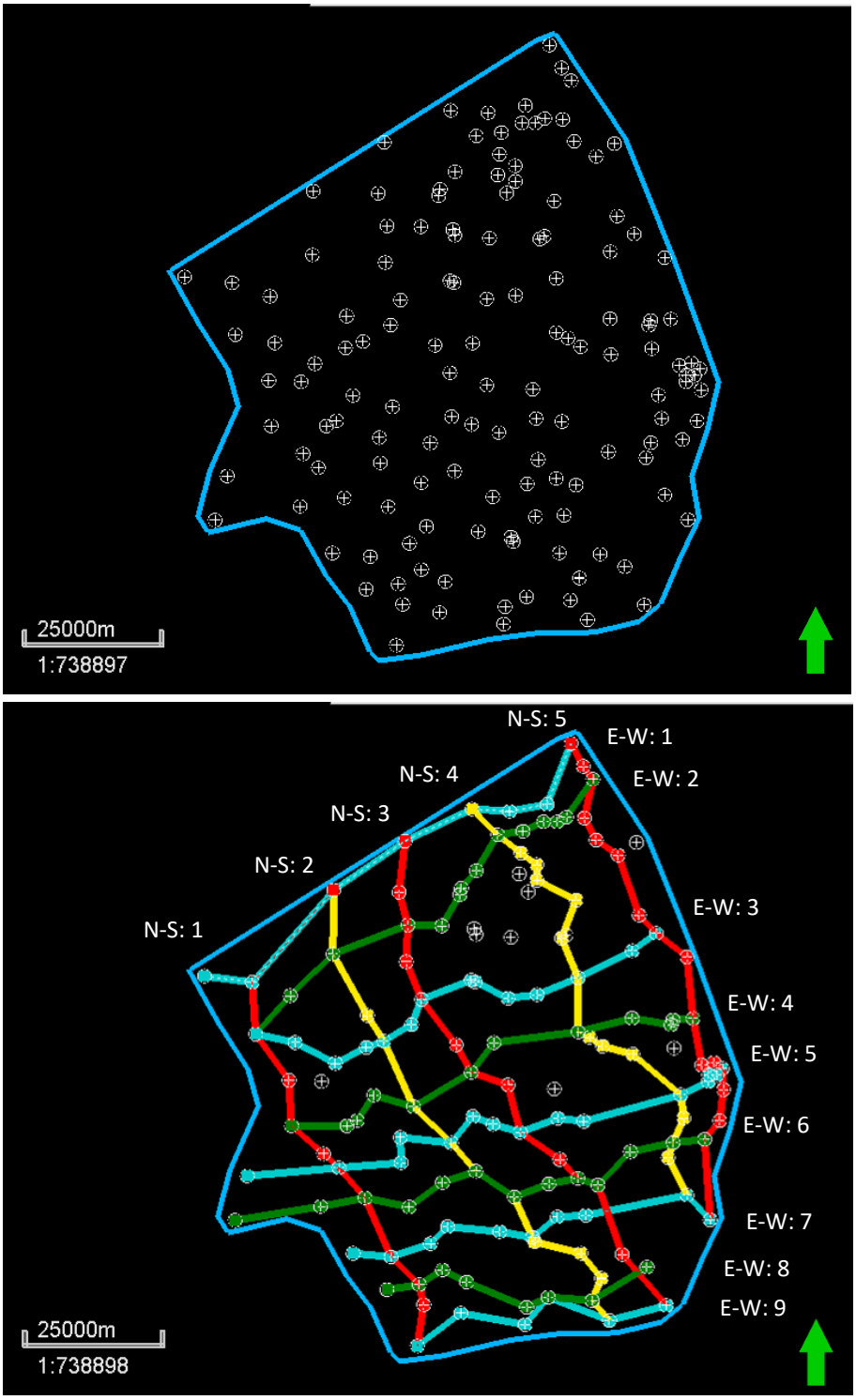

Figure 6. Outlined study area with well header locations for all 141 wells. 14 cross section locations for North to South and East to West trending well sections.

Both models of the handheld XRF devices were calibrated to the Dual Mudrock Air setting where major and trace elements were sequentially collected for a 15 second count and 30 second count respectively. The devices were positioned face down on the slabbed core to scan flush on the core's surface. On sections where data collection was not ideal, special care was taken to position the apparatus away from fractures and other imperfections to collect the most accurate reading while keeping radiation exposure as low as reasonably achievable. On core intervals where plugs were collected, the XRF devices were positioned close to the plug to allow for easy comparisons between elemental distributions and TOC calculations, while still maintaining data integrity.

The elemental data that was collected was output to a table database along with depth, run time, and a standard deviation of error for each individual elemental measurement. The following elemental concentrations were gathered for both models of the Bruker handheld XRF device: Mg, Al, Si, P, S, K, Ca, Ti, Fe, V, Cr, Mn, Co, Ni, Cu, Zn, As, Rb, Sr, Y, Zr, Nb, Mo, Ba, Pb, Th, and U. For elemental concentrations below the instrument's level of detection, concentration was assumed negligible and assigned a null value.

3.3 Core Description and Chronostratigraphy

A detailed core description of Well-X was recorded with the help of Apache Corporation's senior geologist, Brian Coffey. Segments of similar lithology were parceled out by depth and described according to color, dominant lithology, grain size, fossil type, fossil abundance, fossil size, bioturbation index, ultraviolet light response, sedimentary structures, and homogeneity. Three ash bed samples were taken from different sections along Well-X and were dated by

$^{238}U/^{206}P$ system on a Thermal Ionization Mass Spectrometer (TIMS) by Brent Miller of Texas A&M University.

3.4 Correlation Methods and Mapping

All correlations, cross sections, and maps were created using Petrel 2019, a Schlumberger™ software. Key sequence stratigraphic and chemostratigraphic surfaces were correlated across the outlined study area, providing a sequence stratigraphic framework for the Austin Group within Giddings Field. Following the nomenclature patterns of Donovan's previous work, stratigraphic surfaces within this Cretaceous section were first defined with the letter "K" and were then enumerated from 700-800, with older surfaces being assigned smaller values and younger surfaces assigned higher values. Accordingly, the Austin Group is bounded by the K720sb at its base and the K800sb at the top (Donovan, 2019).

4. RESULTS

XRF data collected from Well-X of Brazos County, was crucial in defining the chemostratigraphic and petrophysical relationships within the Austin Group. Figures 7 and 8 display the results from both runs of the handheld XRF devices on Well-X, using the Bruker Tracer 5g and the Bruker Tracer 5i respectively. Both models of the XRF device had very similar distributions for all elements collected in the runs. However, given the high carbonate content of the Austin Chalk, and the Bruker 5g's superior calcium resolution, special emphasis was placed on the 5g's results when selecting surfaces within the Austin Group.

In this study, the Austin Group was divided into a Lower Austin Formation and an Upper Austin Formation, with the boundary between the two occurring along a regionally mappable surface termed the K750sb. The Lower Austin Formation of this study, in general, corresponds to the Lower Chalk of Horovika and Nance (2014). In Well-X (Figures 7 and 8) this boundary corresponds to a distinct increase in the more terrigenous prone elements (e.g., Silicon, Aluminum, Titanium, Potassium, Iron, Zirconium, and Rubidium) from the Calcium-rich lower member of the Austin Group. Another surface (Figures 7 and 8), labeled the K730mfs, was used to further subdivide the Lower Austin Formation into a lower member and upper member. This maximum flooding surface corresponds to an ash bed in Well-X, which is denoted by a regionally mappable high gamma-ray marker. The age of this ash bed is 88.37 Ma $\pm$ 0.22 Ma determined by TIMS dating. The interpreted K750mfs, much like the K730mfs, corresponds to an ash bed in Well-X, which is also denoted a regionally high gamma ray marker, aged 86.8 Ma by TIMS dating. This sample contained many detrital and xenocrystic zircons which made its age difficult to determine. The last surface distinguished in this study, the K760mfs, sub-divides the terrigenous-rich Upper

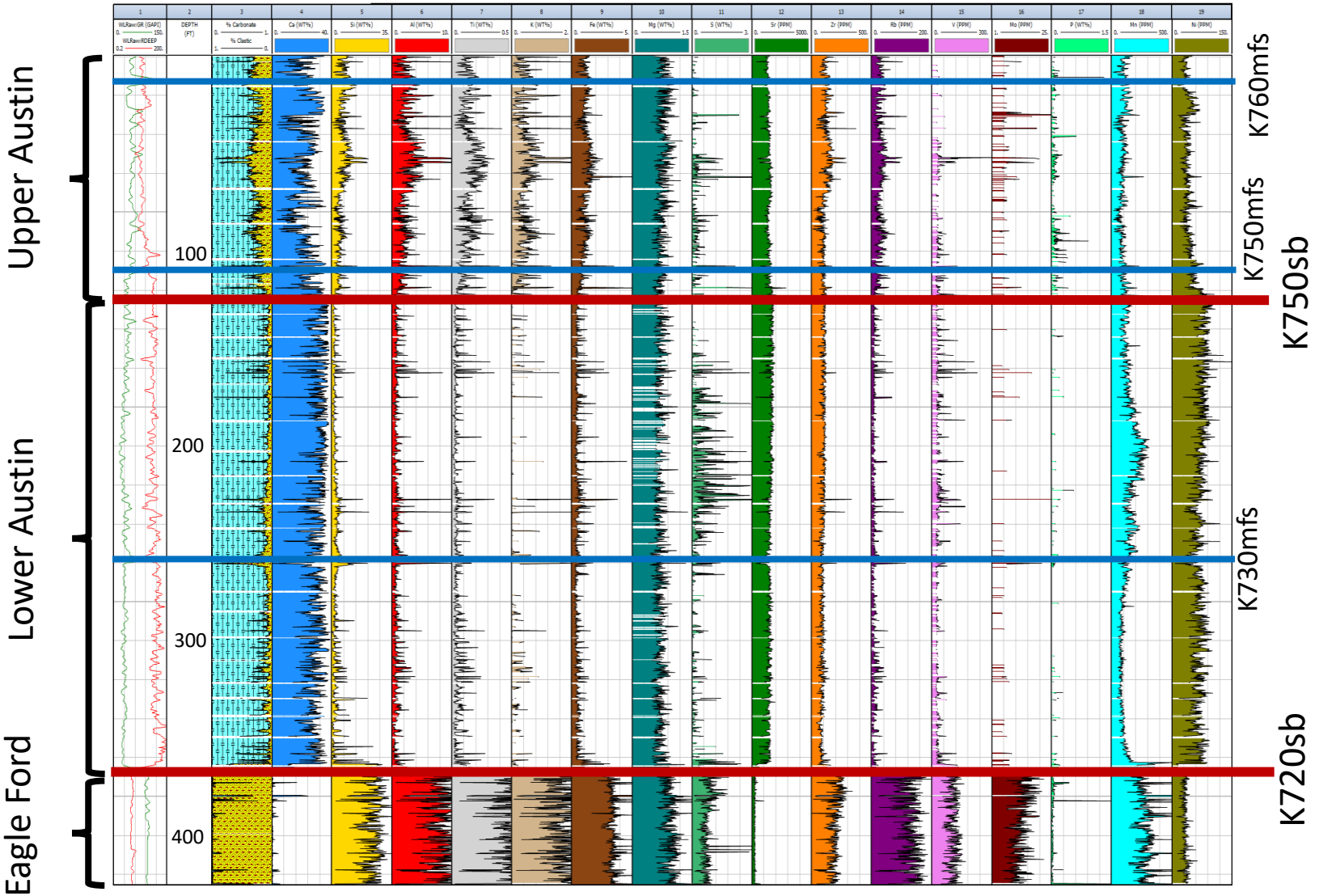

Figure 7. Elemental distribution of cored Well-X section by element using the Bruker Tracer 5g. Sequence boundaries and maximum flooding surfaces marked with red and blue lines respectively. Upper and Lower Austin Formations marked.

Figure 8. Elemental distribution of cored Well-X section by element using the Bruker Tracer 5i. Sequence boundaries and maximum flooding surfaces marked with red and blue lines respectively. Upper and Lower Austin Formations marked.

Austin Formation into a lower and upper member. The K760 maximum flooding surface, like the previously aforementioned maximum flooding surfaces, was selected on a regionally high gamma ray marker/ash bed, which was dated by TIMS at 85.19 Ma $\pm$ 0.19 Ma. A regional sequence boundary the K760sb sits below this marker. Type logs with the complete petrophysical log run of the Austin Group, using the boundaries outlined, and defined by the XRF data from Well-X, are outlined in Figure 9. These type wells were used to correlate the key boundaries across the study area and are representative of the most common logs seen in this study.

The surfaces picked from the petrophysical logs and chemostratigraphic data were correlated across the study area. Figure 10 shows a typical east to west oriented cross section with the thickest Austin Group towards the east and west and a much thinner Austin Group in the center. In this cross section alone, the Austin Group thins from roughly 680 feet at its thickest to 110 feet at its thinnest, a 570-foot difference. Most notably, Figure 10 suggests a surface (K760sb), below the K760mfs that truncates the Lower Member of the Upper Formation, accounting for dramatic thickness changes of that unit. Two datums were used for this cross section, the K720sb or the Base Austin Chalk and the K800sb, the Top Austin Chalk. Cross section A, datumed on the basal K720sb, gives the top of the Austin Group a channelized appearance. Alternatively, cross section B, datumed on the top of the Austin, indicates the underlying Austin truncation is due to an angular unconformity. All cross sections are included in Appendix A.

As illustrated on Figure 11, within the study area, the Austin Chalk had a deepening trend to the southeast. Structure maps of the Top and Base of the Austin Group were generated and both maps showed the same northwest to southeast trend. At its shallowest point in the study area, the K800sb, the Top Austin marker, has a sub-sea total vertical depth, SSTVD, of 180 feet, and at its deepest the same marker has a SSTVD of 11,920 a difference of 11,740 feet. The K720sb, the

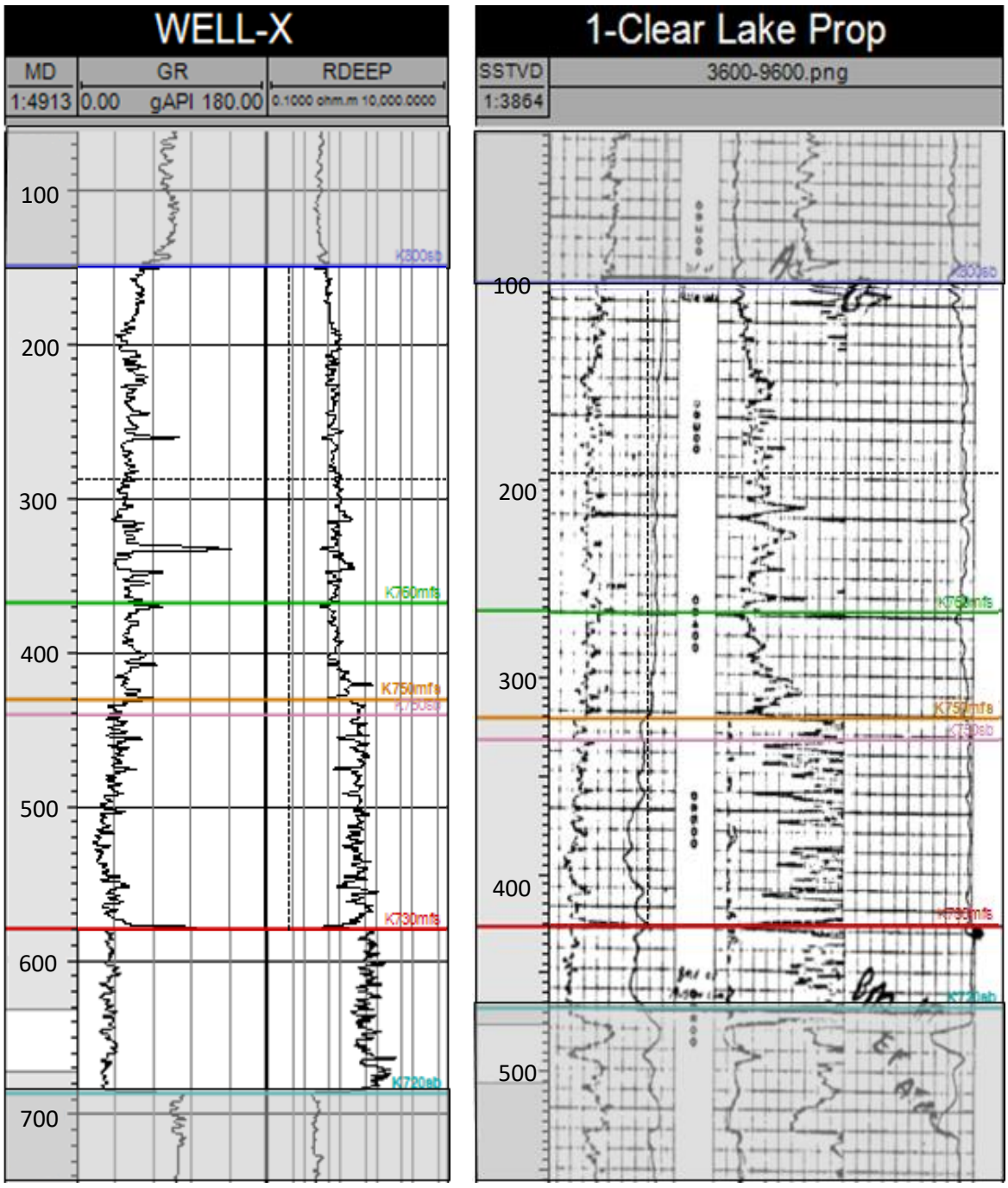

Figure 9. Type logs used in the study area highlighting key stratigraphic sequences. Well-X shows a typical log run in most .las files with a gamma ray and resistivity curve. 1-Clear Lake Prop well shows typical log run in most bitmap images with gamma ray, resistivity, and spontaneous potential curves. Defined lithostratigraphic units marked in Well-X.

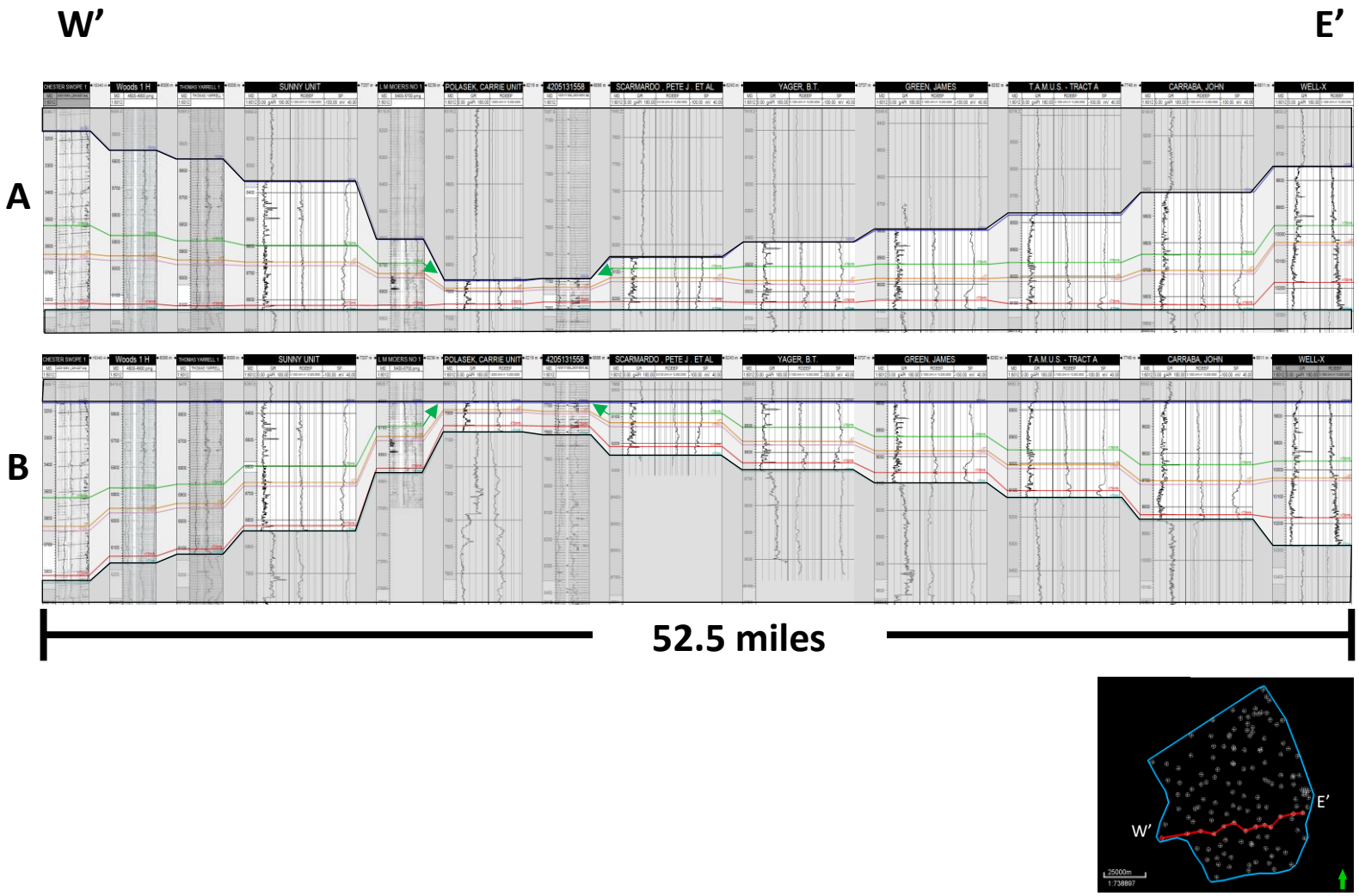

Figure 10. E-W: 6 cross section hung on the Top and Base Austin Chalk. This west to east cross section begins in Burleson County and ends in Brazos County. The Austin Group rapidly thins towards the center of the study area with the thickest sections towards the far east and west. The K760mfs truncates towards the thin.

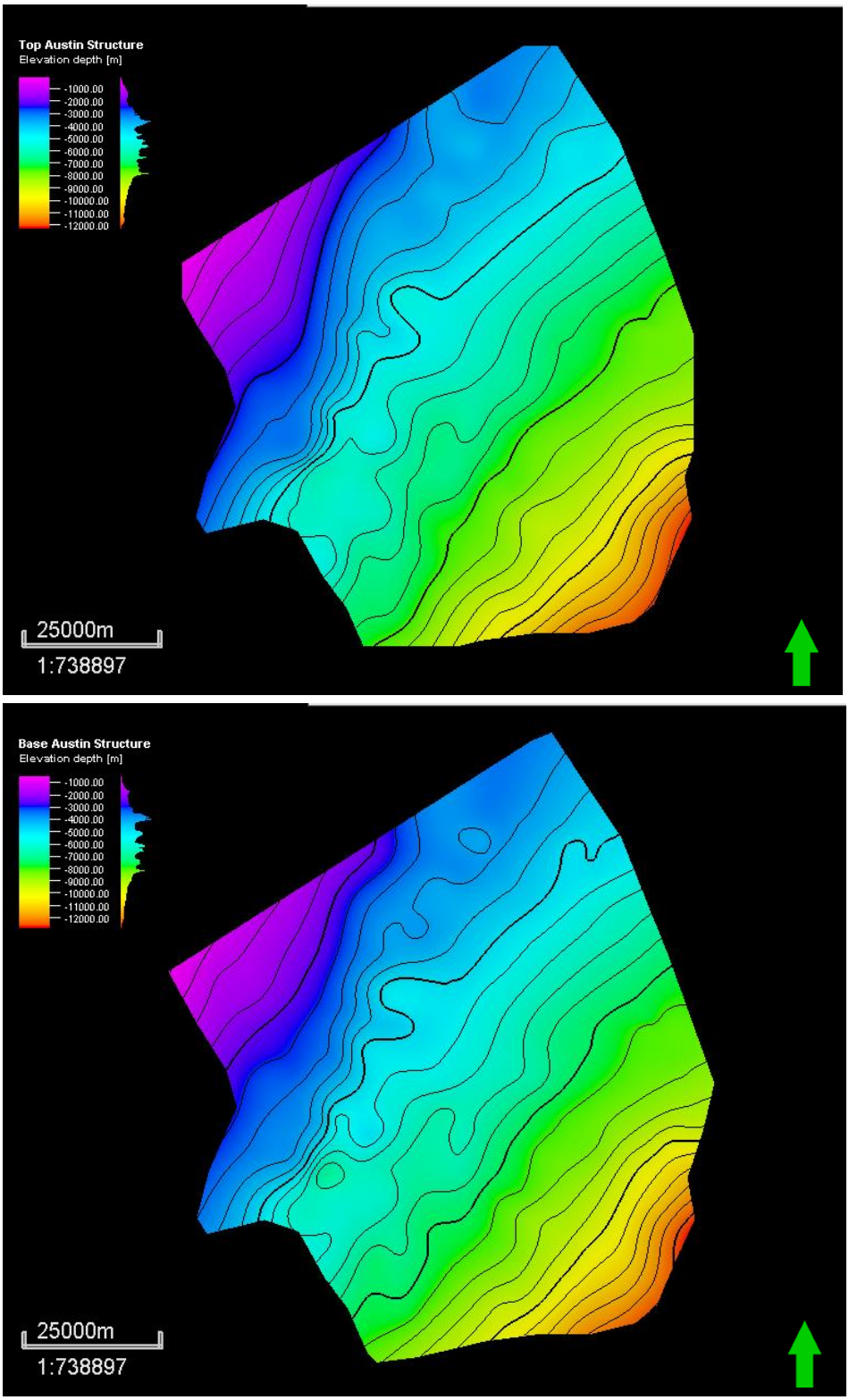

Figure 11. Structure map of the Top and Base Austin Group depicting a deepening trend from the northwest to the southeast.

Base Austin marker, followed the same trend almost identically with a rough total difference in depth of 11,630 feet from the northwest to the southeast.

The Lower Member of the Lower Austin Formation, lying below the K730mfs within this study, is the primary target zone for most drilling ventures in the Austin Chalk. Accordingly, more desirable drilling locations requires greater thicknesses, allowing ample room for multi-stage horizontal drilling activities to exploit this unit. Average thickness of the lowermost unit is roughly 20 to 40 feet, with the thickest section, as seen in the outlined study area (Figure 12), being towards the southeast, and the thinnest section in the northwest. This trend parallels the trend seen in Figure 11's structure maps of the Top and Base Austin markers.

The Austin Group in this study was subdivided into a Lower Austin Formation (LAF) and an Upper Austin Formation (UAF) at the K750sb. As seen in figures 7 and 8, the Lower Austin Formation is more calcium rich with intermittent pulses of argillaceous shales, whereas the Upper Austin Formation is more terrigenous rich. The isopach map of the Lower Austin Formation (Figure 13) shows the thickest part of this unit in the southeast portion of the study area, similar to the previous figures. However, this trend continues further south and wraps around the study area in the west. Significant thinning occurs toward the center of the map where Figure 10 shows a substantial reduction in the total Austin Group thickness. The isopach map of the Upper Austin Formation (Figure 14), shows a similar central thinning oriented north to south with thicker areas towards the east and west. Average thickness for the Upper Austin Formation ranges from 100 to 200 feet, whereas the thickest portion of the Upper Austin Formation is 575 feet in the west, along an approximate north to south trend. The Lower Austin Formation had significantly less thickness variations than the Upper Chalk Formation and, in general, has more uniformly thick internal upper and lower members. The total Austin Group isopach map shows thickness trends (Figure 15)

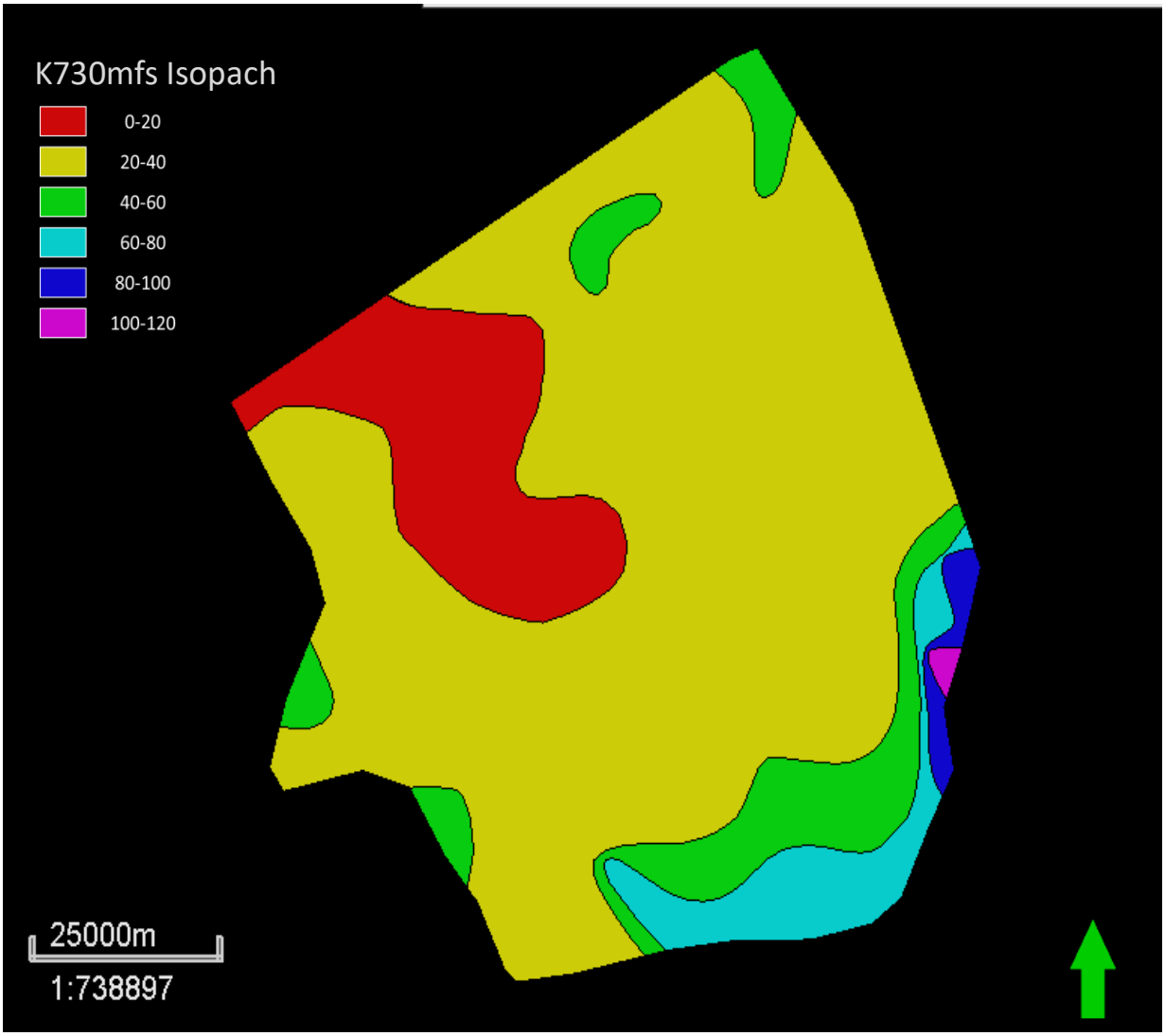

Figure 12. Isopach map of the Lower Member of the Lower Austin Formation, (K720sb – K730mfs). This unit exhibits a thickening trend from the northwest to the southeast.

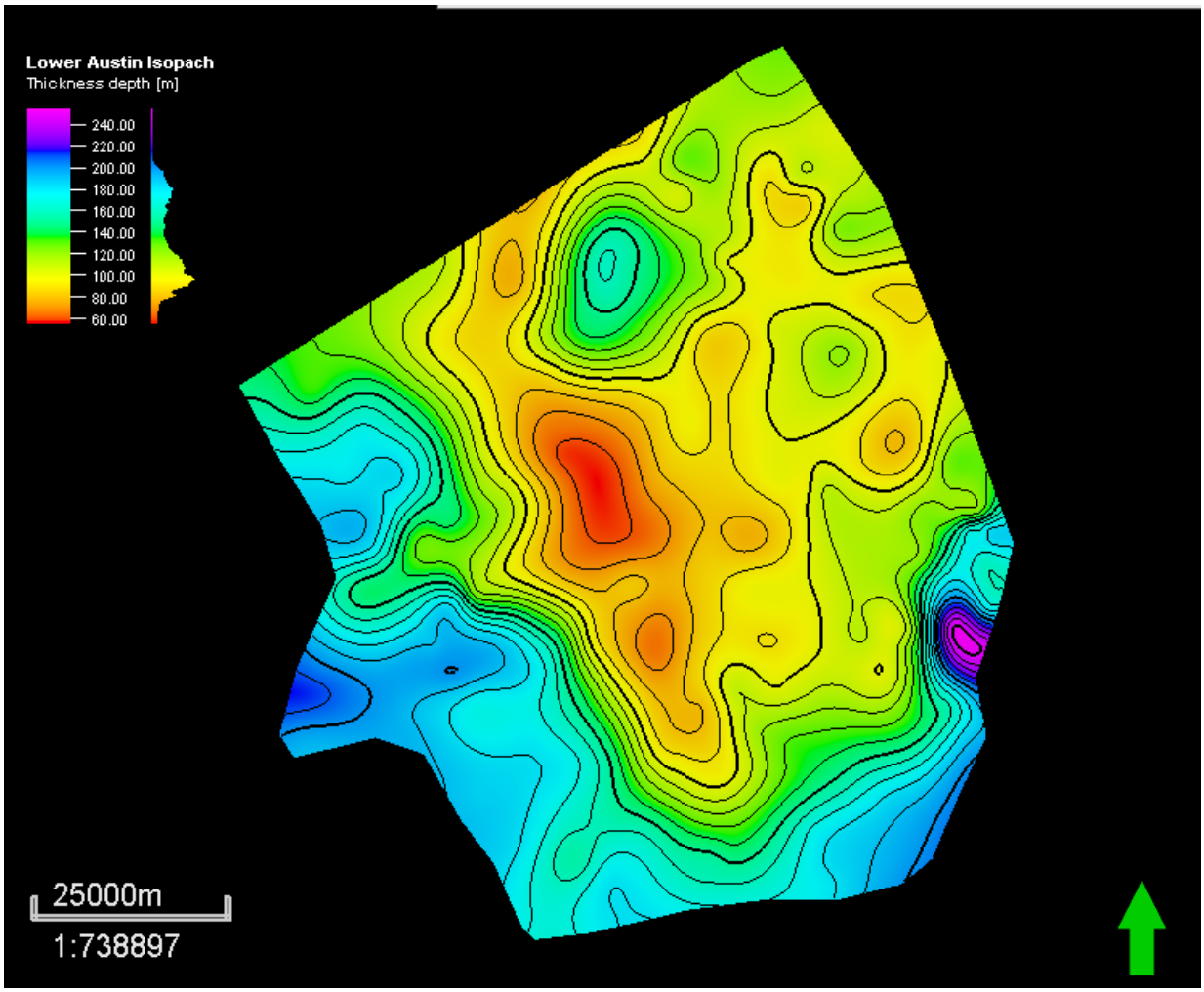

Figure 13. Isopach map of the Lower Austin Formation (K720sb – K750sb). This map exhibits a central thin and a localized thick in the southeast.

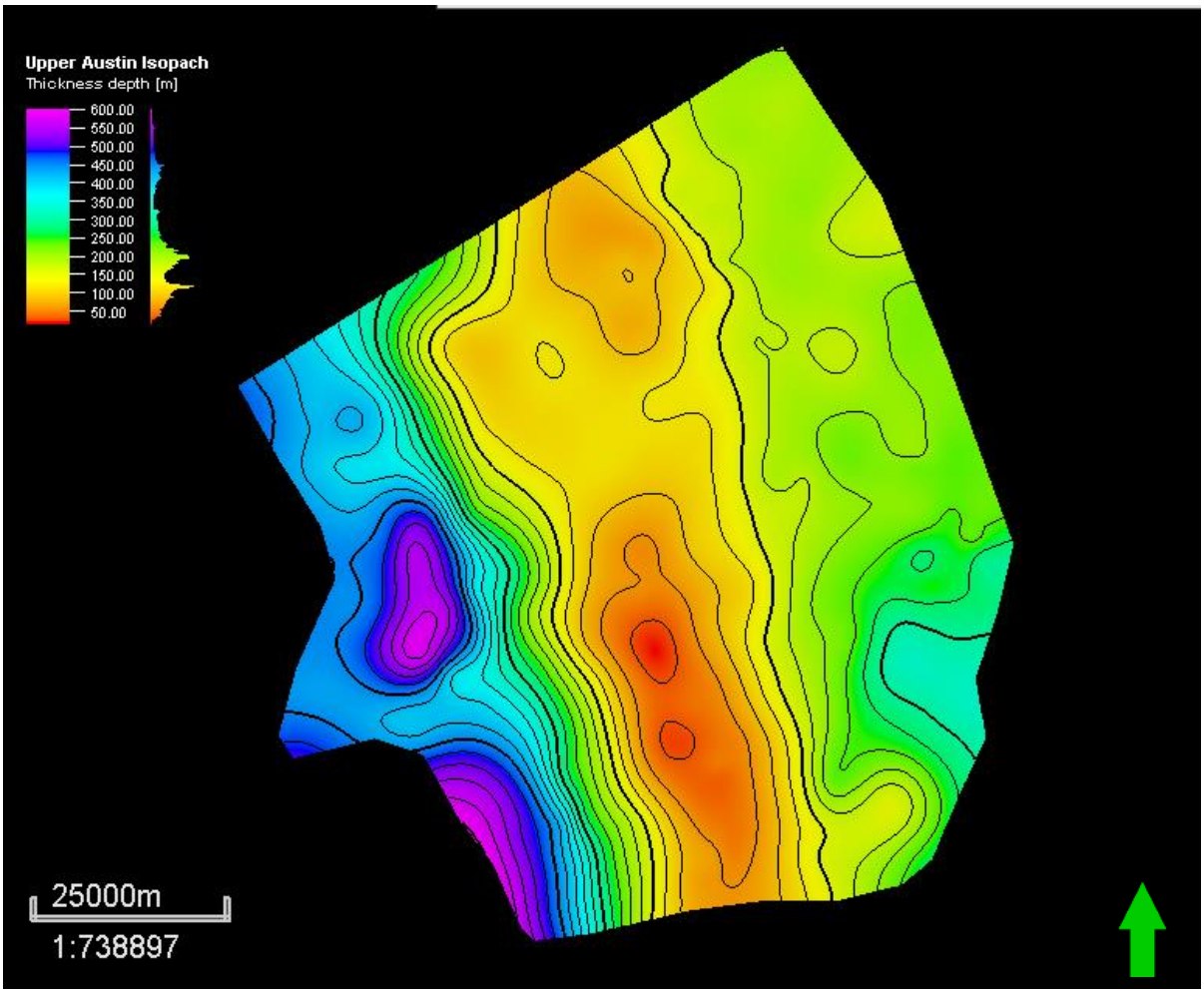

Figure 14. Isopach map of the Upper Austin Formation (K750sb-K800sb). Depicts a central north to south oriented stratigraphic thin with stratigraphic thick sections towards the east and west oriented similarly.

similar to those of the Upper Austin Formation, the total Austin Group has a north to south oriented thin in the center with the thickest portion in the west, which appear to almost exactly overlap with the thickness maps of the Upper Austin Formation. Average thickness of the Austin Group is roughly 300 feet with the thickest and thinnest sections reaching approximately 750 feet and 100 feet respectively. Core photo boundaries are included in Appendix A.

The formation overlying the Austin Chalk, the Taylor Group, was mapped across the study area, and an isopach map of the Taylor Group to the K800sb was generated (Figure 16). This map shows an inverse thickness relationship to that of underlying Austin Group (Figure 15). There is a north to south oriented thick in the center of the study area with the relatively thinnest portions of the Taylor Group oriented similarly in the east and west. This stratigraphic thick directly overlies the total Austin Group's stratigraphic thin. At its thickest, the Taylor Group reaches roughly 1,270 feet compared to 440 feet at its thinnest.

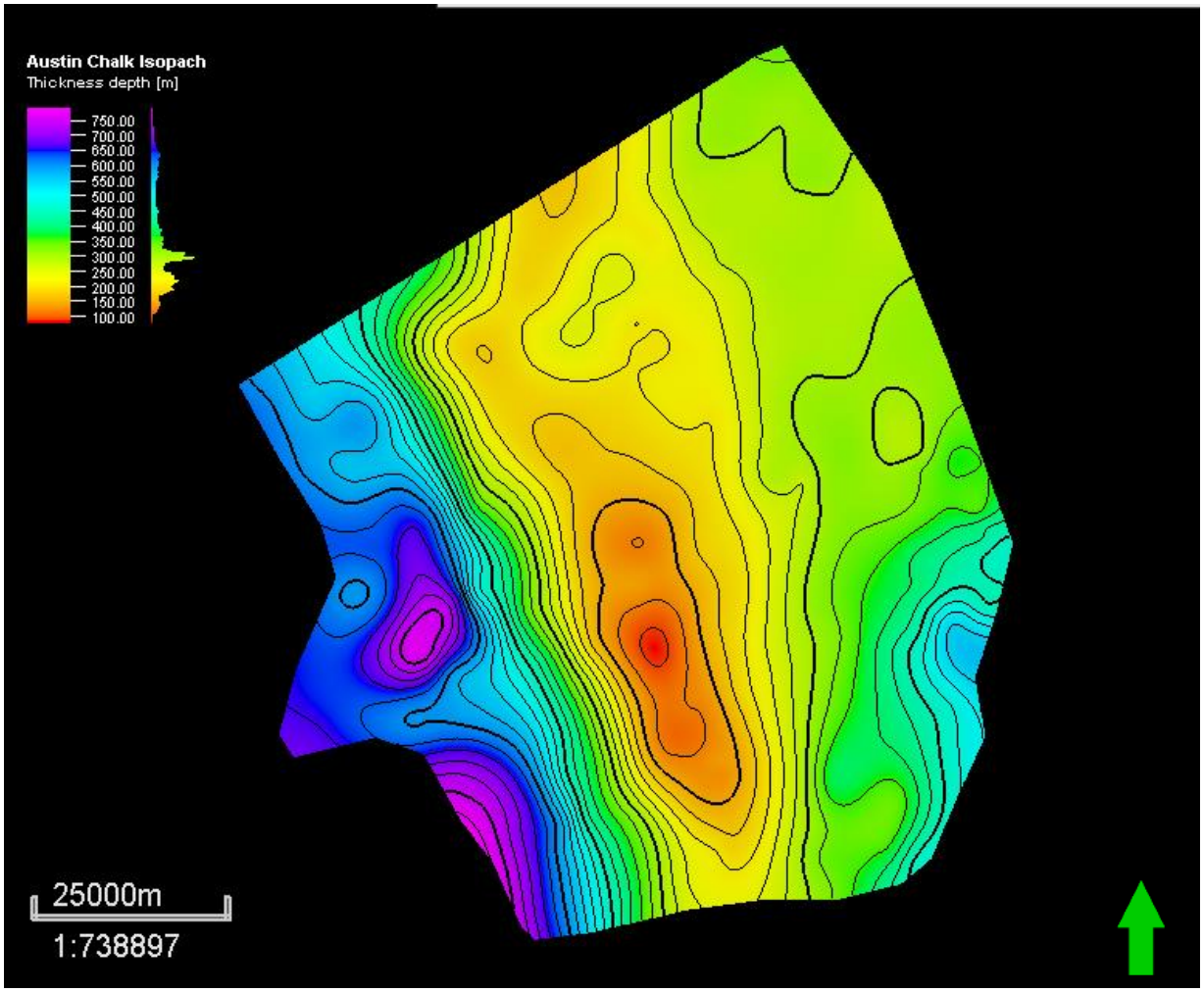

Figure 15. Isopach map of the total Austin Group (K720sb-K800sb). Depicts a central north to south oriented stratigraphic thin with stratigraphically thick sections towards the east and west oriented similarly.

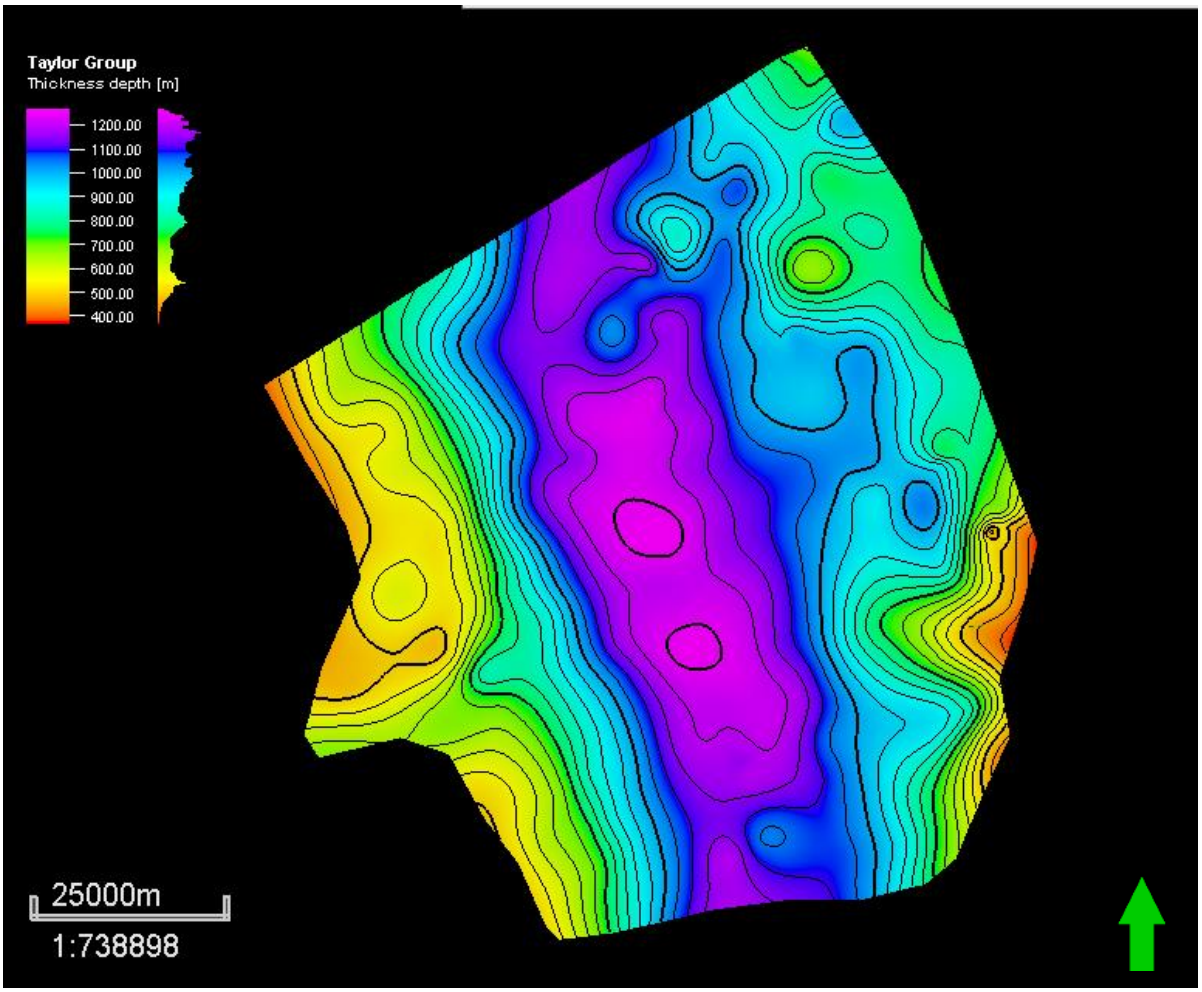

Figure 16. Isopach map of the overlying Taylor Group. Depicts a central north to south oriented stratigraphic thick with stratigraphically thin sections towards the east and west oriented similarly.

5. DISCUSSION

5.1 Chemostratigraphy

Both runs of the Bruker handheld XRF devices yielded differing concentrations of the major and trace elements. The Bruker 5g results showed a visible difference in the calcium resolution from the Bruker 5i. This is likely due to the calibration settings of both models of the handheld devices with respect to their calcium detection. The 5i was intended for everyday point and shoot testing and the 5g was intended for use on more carbonate-rich rocks making the 5g ideal for data collection in the Austin Group. Thus, its results were used to determine key stratigraphic boundaries in Well-X's core.

The chosen elemental curves shown in Figures 7 and 8 are most representative of the overall mineralogy of the Austin Group, and are used to interpret its depositional history. The collected XRF data over the Austin Group reveals key elemental concentrations suggesting oxic bottom-water conditions with little or no upwelling (Table 1). As outlined in Table 1, high concentrations of Nickle, Vanadium, and Manganese suggest substantial organic matter and micronutrient availability common for oxic bottom water conditions with an affinity towards calcium carbonate at the time of deposition (Figures 7 and 8). Nickle behaves as a micronutrient for microbial scavengers and is recorded to have higher concentrations in the carbonate-rich Lower Austin Formation when compared to the more terrigenous-rich Upper Austin Formation (Figures 7 and 8). This falls in line with the core description of a more heavily bioturbated *Inoceramid* rich Lower Austin Formation (Figures 7 and 8). Iron is also a good proxy for characterizing the oxygenation of paleo-oceanographic conditions during the time of deposition (Table 1). Iron shows

	Mineralogy	Proxy	References	Interpretation
Al	Clay minerals. Illite clay group: Glaconite $(K,Na)(Fe^{3+},Al,Mg)_2(Si,Al)_4O_{10}(OH)_2$	Clay and Feldspar	Pearce & Jarvis (1992); Tribovillard *et al.* (2006)	Concentration of clay and feldspars in limestones can be used to help identify sections of clay input and interbedded marls.
Ca	Calcite ($CaCO_3$), Calcium orthophosphates ($CaPO_4$)	Carbonate source and Phosphate accumulation	Banner (1995); Tribovillard *et al.* (2006)	Calcium is primarily a proxy for calcite and calcareous input in limestones.
Si	Quartz (SiO_2)	Quartz	Pearce & Jarvis (1992); Sageman & Lyons (2004)	Silica is used as a proxy for quartz and terrigenous input.
Ti	Detrital sediments (Ti^{4+}, Rutile (TiO_2), and Ti-bearing minerals)	Continental source and dust fraction; Intensity of chemical weathering	Calvert & Pedersen (1993); Zabel *et al.* (2001); Sageman & Lyons (2004)	Titanium and other detrital elements are used as proxies to interpret depositional processes, like source origin and weathering, versus paleooceanographic conditions
Ni	$NiCO_3$, Ni^{2+}, $NiCl^+$ (oxic conditions) NiS (sufate reducing conditions)	Organic matter/micronutrient availability in the water column	Tribovillard *et al.* (2006)	Ni is soluble in oxygenated, marine water columns and behaves as a micronutrient for microbial scavengers. In stratified water columns or in areas of upwelling, scavengers will ingest Ni in oxygenated surface waters and upon death will be deposited and preserved at the anoxic sediment-water interface
Fe	Pyrite (FeS2), Ferroan Dolomite $(Ca(Mg,Fe)(CO_3)_2)$, Siderite ($FeCO_3$)	Redox sensitive	Tribovillard *et al.* (2006)	Trace metals that are redox sensitive are useful for characterizing oxic/suboxic/anoxic paleooceanographic conditions during time of deposition.
S	Pyrite (FeS_2)	Redox sensitive	Tribovillard *et al.* (2006)	Trace metals that are redox sensitive are useful for characterizing oxic/suboxic/anoxic paleooceanographic conditions during time of deposition.
P	Phosphates Apatite($Ca_5(PO_4)_3(Cl/F/OH)$)	Phosphate accumulation; Upwelling	(Tribovillard *et al.* (2006)	PO_4^{3-} is released from decaying organic matter. However, it can either escape back to the water column or be trapped within the depositing sediment. Thus, it is not an independently reliable productivity/upwelling or redox proxy, but can be used in conjunction with multiple proxies.
Mn	MnO_2, Mn^{2+}/Mn(IV), and Mn(II) oxides	Redox sensitive, Mn-enrichment common during oxic bottom water conditions. Affinity towards calcium carbonate	Calvert & Pedersen (1993); Sageman & Lyons (2004); Tribovillard *et al.* (2006); Brumsack (2006)	The mobile nature of Manganese in reducing conditions allows for ease of transfer of trace metals out of the water column and into the depositing sediment. Upwelling sediments are low in Mn-enrichment.
Sr	Sr-Ca substitutes in calcite, aragonite and dolomite	Carbonate source and phosphate. Affinity towards calcium carbonate	Pratt (1990), Scholle (1977); Renard (1979); Banner (1995); Tribovillard *et al.* (2006)	With an affinity for substitution in carbonate forming minerals, Strontium is used as a proxy for carbonate source and diagenetic influence.
V	HVO2-4 and H2VO-4 (oxic) VO2-, VO(OH)-3, VO(OH)2 (mildly reducing)	Bottom water anoxia, redox sensitive. Authigenic organometallic input	Helz *et al.* (1996); Sageman & Lyons (2004); Tribovillard *et al.* (2006); Algeo and Rowe, 2012	Redox sensitive trace metals help determine paleoceanographic conditions during deposition. Enrichment of Vanadium occurs in suboxic-anoxic conditions because it is immobile in low oxygen, restricted environments.
Ba	Barite ($BaSO_4$)	Paleoproductivity	Robin *et al.* (2003); Griffith & Paytan (2012); Liguori *et al.* (2016)	Barium is found as Barite in the water column and is associated with carbon export flux. In anoxic, sulfate reducing environments, barite is not preserved. Barium can reprecipitate as barite in oxic sediment layers, thus diagenetic alteration must be assessed to use Barium as a reliable proxy.

Table 1. Interpretation and mineralogy of measured elemental concentrations collected from Bruker handheld XRF devices. (McCreary, in prep).

an inverse relationship to Nickle for this core; the Lower Austin Formation has a high concentration of Nickle and low concentrations of Iron when compared to the Upper Austin Formation, which has relatively low concentrations of Nickle and high concentrations of Iron, suggesting oxic conditions.

The Austin Group was divided by the K750sb; the point at which the carbonate-rich Lower Austin Formation was separated from the terrigenous-rich Upper Austin Formation. The Silicon, Aluminum, Titanium, and Potassium curves were used to mark this transition in elemental concentrations of source material and are the prominent lithologic markers of the Upper Austin Formation (Figures 7 and 8). Silicon was used as a proxy to designate zones rich in quartz and other terrigenous materials. Aluminum and Potassium were used as a proxy for clay and feldspar to identify interbedded marly input, and Titanium was used to identify continental source rock material and the intensity of chemical weathering (Table 1). Given the increased concentrations of all four elements above the K750sb, the Upper Austin Formation is interpreted as more terrigenous-rich with more frequent clay-rich interbeds. Conversely, the Lower Austin Formation is more carbonate-rich than the Upper Austin Formation. The Austin Group, being a chalk, is predominately composed of calcium, which is used as a proxy for carbonate sources and phosphate accumulation (Table 1). Overall, the Lower Austin Formation has more homogenous blocky calcium-rich bedsets with only intermittent terrigenous-rich inter-beds.

5.2 Sequence Stratigraphy

Petrophysical logs and the XRF chemostratigraphic data were analyzed together and they resolve four sequence boundaries and three maximum flooding surfaces used to subdivide the Austin Group. The K720sb separates the Austin Group from the underlying Eagle Ford Group,

and the K800sb separates the Austin Group from the overlying Taylor Group. The K750sb separates the carbonate-rich Lower Austin Formation from a more terrigenous-rich Upper Austin Formation. The K760sb, which directly underlies the K760mfs, separates the Lower (LM:UAF) and Upper (UM:UAF) Members of the Upper Austin Formation.

At the K750sb, the blocky calcium-rich unit dramatically decreased in concentration in favor of Silicon, Aluminum, Titanium, Potassium, Iron, Zirconium, and Rubidium. The Lower Austin Formation also has higher resistivity and lower gamma values than the Upper Austin Formation which saw the inverse. Three ash beds with regionally high gamma ray values are interpreted as maximum flooding surfaces (K730mfs, K750mfs, and K760mfs). These ash beds were age dated using the Uranium-Lead method via TIMS. In general, the K750sb and K760mfs respectively coincide with the classic lithostratigraphic base of the Jonah and the base of the Dessau. The K730mfs, was used to divides the Lower Austin Formation into a Lower (LM:LAF) and Upper (UM:LAF) member. The LM:LAF Formation is the primary exploitation target for hydrocarbon recovery due to its proximity to the Eagle Ford Group and its homogenous and fewer clay-rich interbeds which are ideal for modern fracing techniques. This interval sees the highest resistivity and lowest gamma ray readings of any other interval (Figures 7 and 8). The UM:LAF is also a blocky carbonate unit, but with an increase in Sulfur and Manganese content from the member below. Additionally, there is an increase in frequency and intensity of terrigenous-rich beds in this unit, suggesting the unit is less homogenous and more clay-rich than the underlying LM:LAF, making it a less than ideal target for fracing despite its higher overall total organic carbon values than seen in other intervals.

The Upper Austin Formation has much higher concentrations of terrigenous elements than seen in the Lower Austin Formation. The UM:UAF is separated from the LM:UAF by the

K760mfs. The UM:UAF does not occur in 11% wells within the study area. All these wells occur within the bounds of the regional thin seen in the isopach maps of the total Austin Group thickness and the Upper Austin Formation thickness (Figures 14 and 15), likely meaning this unit was incised. Unfortunately, due to Well-X's limited coverage of the Upper Austin Chalk Formation, further research is needed to more accurately define the internal chemostratigraphic characteristics, and precise sequence stratigraphic boundaries.

5.3 Waco Channel

As seen in the isopach maps of the Total Austin Group and the Upper Austin Formation, there is a dramatic north to south oriented thinning near the center of the study area (Figures 14 and 15), commonly referred to as the Waco Channel (Durham, 1991), with prominent thickness increases oriented in the same north to south directions to the far east and west. The cross section in Figure 10 is an excellent representation of the typical west to east trend seen in this study area. Figure 10 has two different datums for the same cross section which can change the interpretation of the depositional history of the Austin Group. Cross section A, hung on the Base of the Austin Group (K720sb), shows the channelized appearance of its top, where the Upper Austin Formation was eroded, accounting for the drastic thinning seen in the middle of the study area. Cross section B, hung on the Top of the Austin Chalk (K800sb) can be interpreted as an angular unconformity, where the Upper Austin Formation located in the middle of the study area was uplifted and eroded.

To determine the manner in which the Upper Austin Formation thinned, this study was expanded, and the overlying Taylor Group was correlated across the study area (Figure 16). The Taylor Group shows a north to south oriented thick measuring approximately 1,200 feet at its thickest in the center of the study area, with similarly oriented thins to the far east and west roughly

500 feet thick. Interestingly, the thickest portion of the Taylor Group falls directly over the thinnest portion of the Austin Group, suggesting an incised channel system, likely the Waco Channel. This channel eroded much of the Upper Austin Group and formed the dramatic thin seen in the center of the study area creating accommodation space for the overlaying Taylor Group to fill upon deposition, making the overlying thick seen in Figure 16. Further evidence of incision is the thickness variations seen in the Upper Austin Formation when compared to the Lower Austin Formation. Much of the Lower Austin is comprised of low relief, homogenously thick internal Lower and Upper members (Figure 13), while the Upper Austin Formation has thickness variations of over 500 feet and is nearly eroded entirely in some portions by the Waco Channel (Figure 14). In fact, approximately 11% of the wells in this study are missing the UM:UAF completely. More detailed correlation of the internal markers within the Taylor Group are needed to approximate the timing of the Waco Channel.

5.4 Petroleum Exploration Significance

Historically, the main target for most drilling ventures in the Austin Group is the LM:LAF. This member is the closest vertical migration upward from the main source component for hydrocarbons in the Austin Group, the Eagle Ford Formation. The LM:LAF is carbonate-rich with few clay interbeds and numerous natural fractures, making it ideal for modern multi-stage fracing techniques. The LM:LAF was deposited in more oxic conditions than the UM:LAF and is more heavily bioturbated (Figure 7 and 8). An isopach map of the LM:LAF was generated to show its thickness variations across the study area (Figure 12). Thickest sections of this member are found in the southeastern portion of the study area, where the Austin Group is also structurally deepest (Figure 11).

There is potential for future drilling activities in the UM:UAF outside of the typical Lower Austin Chalk Play. The Upper Austin Group becomes more limestone prone towards the down dip section where the Upper Austin is incised by the Waco Channel. This could potentially act as a sub-unconformity play where hydrocarbons sub-crop under the canyon. Although, further study of the Upper Austin Formation, especially its chemostratigraphic characteristics, is needed to better define, map, and high-grade this potential play.

6. CONCLUSIONS

The Austin Group in the western side of the East Texas Basin is an interpreted 2nd-order, unconformity bounded, depositional sequence with distinct petrophysical and chemostratigraphic signatures. Significant sequence boundaries and maximum flooding surfaces were correlated across the study area from Well-X to define and map key chemostratigraphic based chronostratigraphic units within the Austin Group. Using the elemental distribution from the Bruker Tracer 5g XRF data and petrophysical logs, the Austin Group is subdivided into a carbonate-rich Lower Austin Formation and a more terrigenous-rich Upper Austin Formation separated by the K750 sequence boundary. The Lower Austin Formation was further subdivided by the K730 maximum flooding surface into a Lower Member and an Upper Member. The LM:LAF is the primary exploitation target for most drilling activities in the Austin Chalk. This interval is thickest in the southeast portion of the study area and tends to be more homogenous with less clay-rich interbeds. These characteristics provide the ideal parameters for multi-stage fracing techniques to penetrate and connect the internal matrix porosity in the LM:LAF and recover hydrocarbons which migrated into the unit from source rocks within the underlying Eagle Ford Group. Similar to the Lower Austin Formation, the Upper Austin Formation was also divided into a Lower and Upper Members by a regionally mappable high gamma ray marker interpreted as a maximum flooding surface, K760mfs.

Within the study area, the Austin Group has a north to south oriented stratigraphic thin truncating the Upper Austin Formation, interpreted as the Waco Channel. This incision eroded much of the Upper Austin Formation, and created large accommodation space for deposition of the overlaying Taylor Group, resulting in a stratigraphically thick Taylor Group being deposited

over the thinnest portion of the Austin Chalk Formation. It should be noted, however, that further study of the Taylor Group is needed to determine the exact depositional history of the Waco Channel.

Finally, although further study of the UM:UAF is needed, due to Well-X's limited core coverage, an additional fractured chalk play may exist within this unit. However, further study of the UM:UAF, especially its chemostratigraphic characteristics, is needed to better define, map, and high-grade this new potential play.

REFERENCES

Adkins, W., 1932, The Mesozoic systems in Texas, in E. H. Sellards, W. S. Adkins, and F. B. Plummer, eds.: The Geology of Texas- University of Texas Bulletin 3232, p. 239-518.

Algeo, T. and H. Rowe, 2012, Paleo-oceanographic applications of trace-metal concentration data: Chemical Geology, v. 324, p. 6–18.

Banner, J., 1995, Application of the trace element and isotope geochemistry of strontium to studies of carbonate diagenesis: Sedimentology, v. 42, p. 805–824.

Blakey, R., 2019, Global Paleogeography: Global Series- Cretaceous.

Brumsack, H.., 2006, The trace metal content of recent organic carbon-rich sediments- Implications for Cretaceous black shale formation: Paleogeography, Palaeoclimatology, Paleoecology, v. 232, p. 344–361.

Calvert, S., and T. Pedersen, 1993, Geochemistry of Recent Oxic and Anoxic Marine Sediments- Implications for the Geological Record. Marine Geology: Elsevier.

Clark, W., 1995, Depositional environments, diagenesis, and porosity of upper cretaceous volcanic-rich Tokio sandstone reservoirs, Haynesville Field, Clairborne Parish, Louisiana. United States Department of Energy.

Dawson, W., and D. Reaser, 1990, Trace fossils and paleoenvironments of lower and middle Austin Chalk (Upper Cretaceous), north-central Texas: Transactions—Gulf Coast Association of Geological Societies, v. 40, p. 161–173.

Donovan, A., S. Gifford, A. Pramudito, M. Meyer, and M Pope, 2019, Unraveling the Secrets of the Eaglebine: URTEC, Unconventional Resource Technology Conference.

Dravis, J., 1979, Sedimentology and diagenesis of Upper Cretaceous Austin Chalk Formation, South Texas and northern Mexico: Houston, Texas, Rice University, PhD dissertation, p. 513.

Durham, C., and S. Hall, 1991, The Austin Chalk - Bed by Bed Through Central Texas: AAPG Data pages and Archives, South Texas Geological Society Special Publications.

Griffith, E., and A. Paytan, 2012, Barite in the Ocean – Occurrence, Geochemistry and Palaeoceanographic Applications: Wiley Online Library, John Wiley & Sons, Ltd.

Hagerty, M., 2018, Magnolia Oil and Gas: Yet Another Deal Offering Production Upside: BTU Analytics, Magnolia Oil and Gas.

Halbouty, M., 1990, East Texas Field-U.S.A., East Texas Basin, Texas, AAPG Special Volume: Stratigraphic Traps II, p. 189-206.

Helz, G., C. Miller, J. Charnock, J. Mosselmans, R. Pattrick, C. Garner, and D. Vaughan, 1996, Mechanism of molybdenum removal from the sea and its concentration in black shales: EXAFS evidence Geochem. Cosmochim. Acta, v. 60 p. 3631-3642.

Hovorka, S., and H. Nance, 1994, Dynamic depositional and early diagenetic processes in a deep-water shelf setting, Upper Cretaceous Austin Chalk, north Texas: Transactions—Gulf Coast Association of Geological Societies, v. 44, p. 269–276.

Jackson, M., and S. Laubach, 1991, Structural History and origin of the Sabine Arch, East Texas and Northwest Louisiana: Texas Bureau of Economic Geology, Geological Circular, p. 47.

Laurentian Research, 2019, Austin Chalk Revived- An Emerging Unconventional Play: Seeking Alpha, The Natural Resource Hub.

Liguori, B., M. Almeida, and C. Rezende, 2016, Barium and Its Importance as an Indicator of (Paleo)Productivity: Anais Da Academia Brasileira De Ciências, Academia Brasileira De Ciências.

Loucks, R., and S. Peng, 2021, Matrix Reservoir Quality of the Upper Cretaceous Austin Chalk Group and Evaluation of Reservoir-Quality Analysis Methods; Northern Onshore Gulf of Mexico, U.S.A: Marine and Petroleum Geology, Elsevier.

McCreary, M.., in Prep. Chemostratigraphic and Sequence Stratigraphic Analysis of the Austin Chalk in the Outcrops and Subsurface of Texas: Texas A&M University.

O'Connor, L., S. Robinson, D. Naafs, and H. Jenkyns, 2019, Late Cretaceous Temperature Evolution of the Southern High Latitudes- A TEX 86 Perspective: AGU Journals, John Wiley & Sons, Ltd.

Parshall, J., 2017, Momentum Gathers for Austin Chalk Revival: Society of Petroleum Engineers, Journal of Petroleum Technology.

Pearce, T., and I. Jarvis, 1992, Applications of geochemical data to modelling sediment dispersal patterns in distal turbidites- Late Quaternary of the Madeira abyssal plain: Journal of Sedimentary Petrology, v. 62, p. 1112–1129.

Pearson, K., and R. Dubiel, 2011 Assessment of Undiscovered Oil and Gas Resources of the Upper Cretaceous Austin Chalk and Tokio and Eutaw Formations, Gulf Coast- National Assessment of Oil and Gas Fact Sheet: USGS: Science for a Changing World.

Pearson, K., 2012, Geologic models and evaluation of undiscovered conventional and continuous oil and gas resources—Upper Cretaceous Austin Chalk, U.S. Gulf Coast: U.S. Geological Survey Scientific Investigations Report 2012–5159, p. 26.

Pratt, L., E. Force, and B. Pomerol, 1990, Coupled Manganese and Carbon-Isotopic Events in Marine Carbonates at the Cenomanian-Turonian Boundary: Pennsylvania State University, Journal of Sedimentary Petrology.

Renard, M., G. Richebois, and R. Letolle, 1979, Strontium, Manganese, and Iron Contents, and Oxygen Isotopes in the Carbonate Fraction Recovered from Hole 398C, Leg 47B: Universite Pierre et Marie Curie Laboratoire De Géologie Des Bassins Sédimentaires.

Robin, E., C. Rabouille, G. Martinez, I. Lefevre, J. Reyss, P. VanBeek, and C. Jeandel, 2003, Direct barite determination using SEM/EDS-ACC system- implication for constraining barium carriers and barite preservation in marine sediments: Marine Chemistry v. 82, p. 289-306.

Sageman. B., and T. Lyons, 2004, Geochemistry of fine-grained sediments and sedimentary rocks. In: Mackenzie, F. (ed.) Sediments, Diagenesis, and Sedimentary Rock: Treatise on Geochemistry, 7. Elsevier, Amsterdam, p. 115–158.

Scholle, P., 1977, Chalk Diagenesis and Its Relation to Petroleum Exploration- Oil from Chalks, a Modern Miracle: AAPG Bulletin, American Association of Petroleum Geologists.

Shumard, B., 1860, Observations upon the Cretaceous strata of Texas: Academy of Science St. Louis, Transactions v.1, p. 582-590.

Stanley, S., and J. Luczaj, 2015, The Cretaceous World.: Earth System History, 2nd ed., W.H. Freeman and Company, a Macmillan Higher Education Company, p. 417–445.

Tribovillard, N., J. Thomas, T. Lyons, and R. Armelle, 2006, Trace metals as paleo-redox and paleo-productivity proxies- An update: Chemical Geology v. 232: p. 12-32.

Young, K., 1977, Guidebook to the Geology of Travis County. The Student Geology Society, The University of Texas.

Zabel, M., R. Schneider, T. Wagner, A. Adegbie, U. Vries, and S. Kolonic, 2001, Late Quaternary climate changes in central Africa as inferred from terrigenous input to the Niger fan: Quaternary Research., v. 56, p. 207–217.

Zuckerman, G., 2014, The Frackers: Penguin Group, New York, p. 747.

APPENDIX A

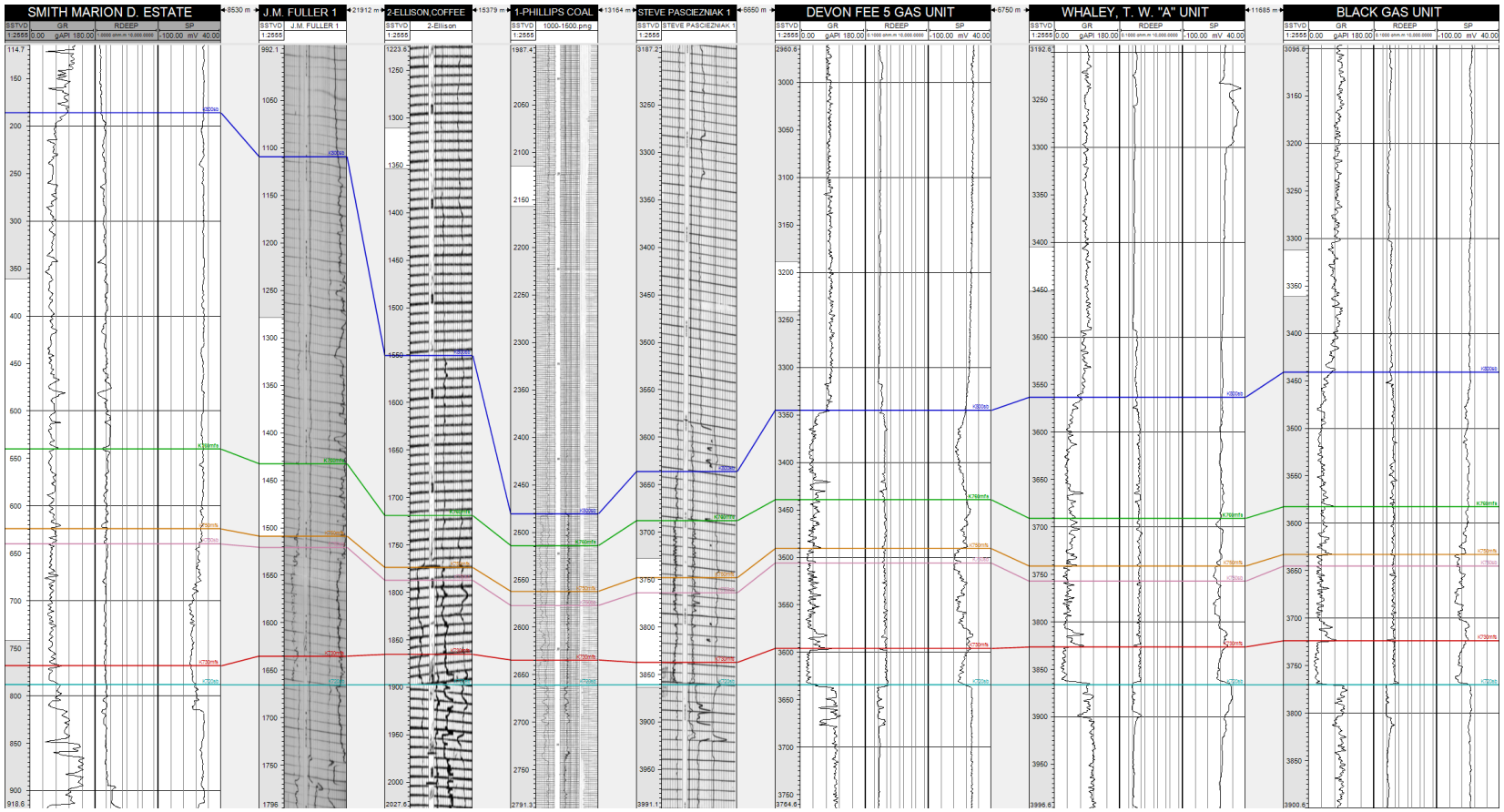

Figure A1. Cross section E-W: #1. West to East oriented cross section of the Austin Group with internal sequence boundaries and maximum flooding surfaces .

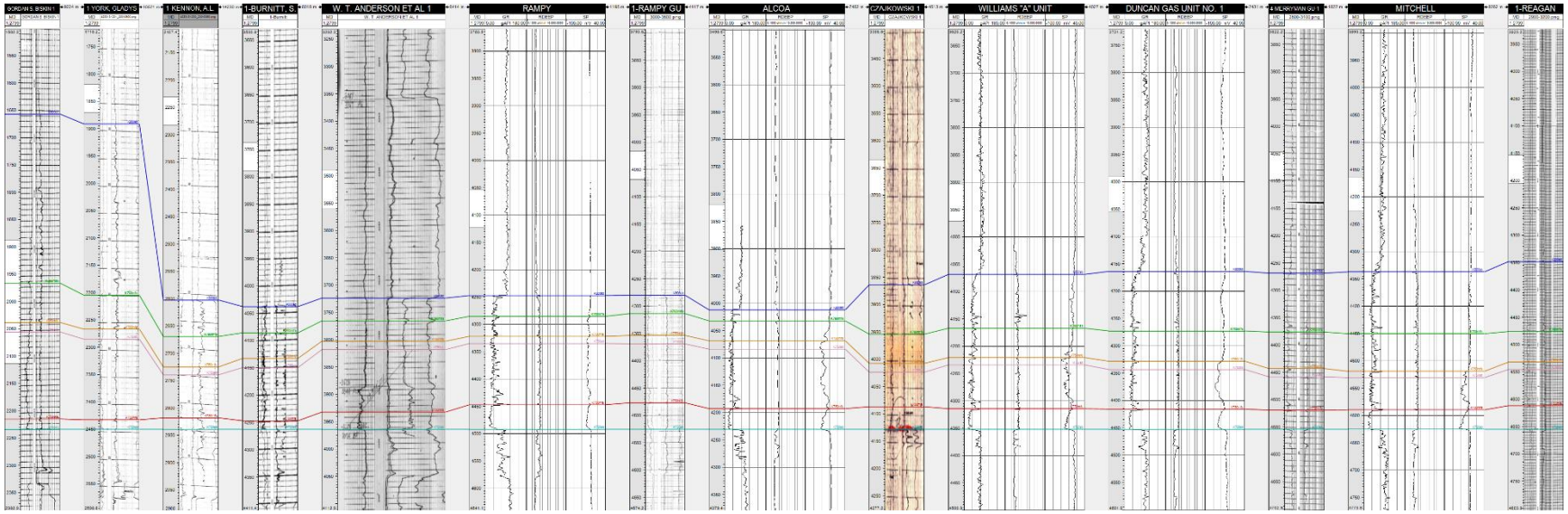

Figure A2. Cross section E-W: #2. West to East oriented cross section of the Austin Group with internal sequence boundaries and maximum flooding surfaces .

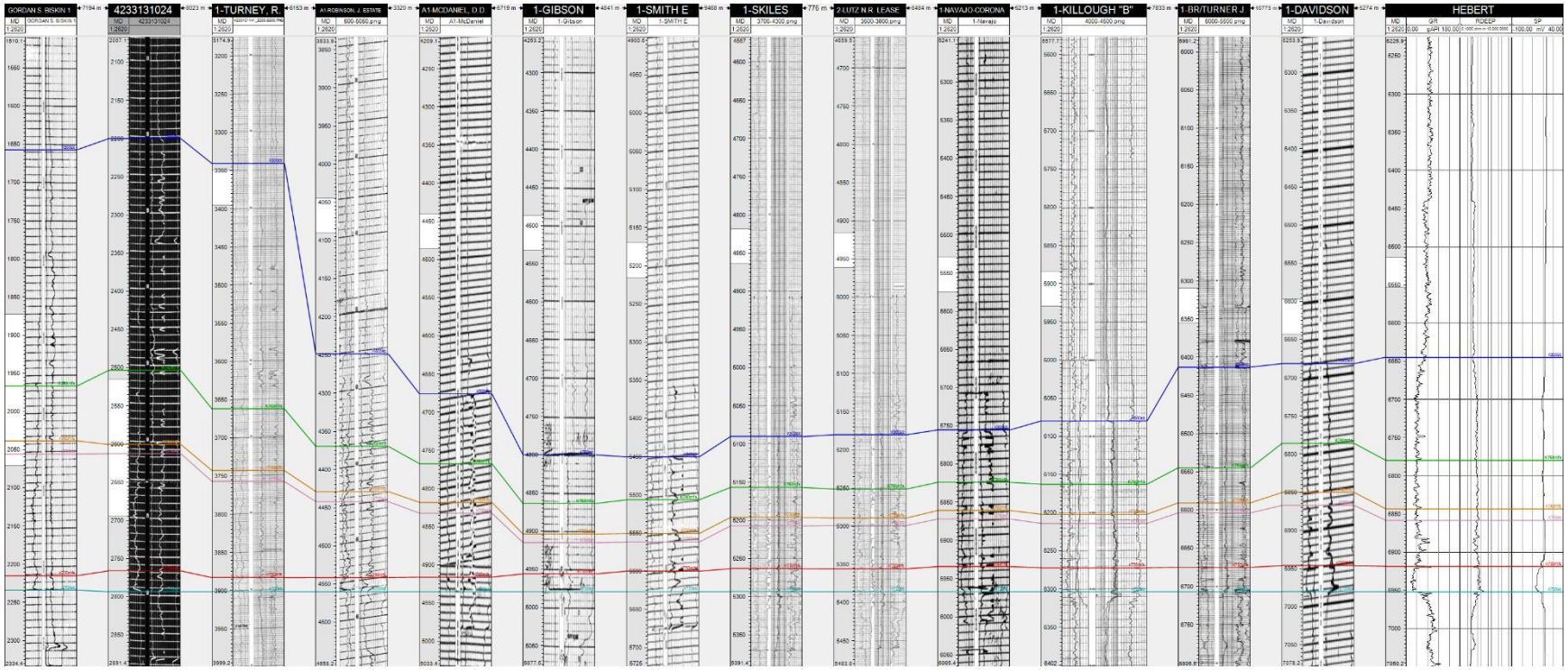

Figure A3. Cross section E-W: #3. West to East oriented cross section of the Austin Group with internal sequence boundaries and maximum flooding surfaces .

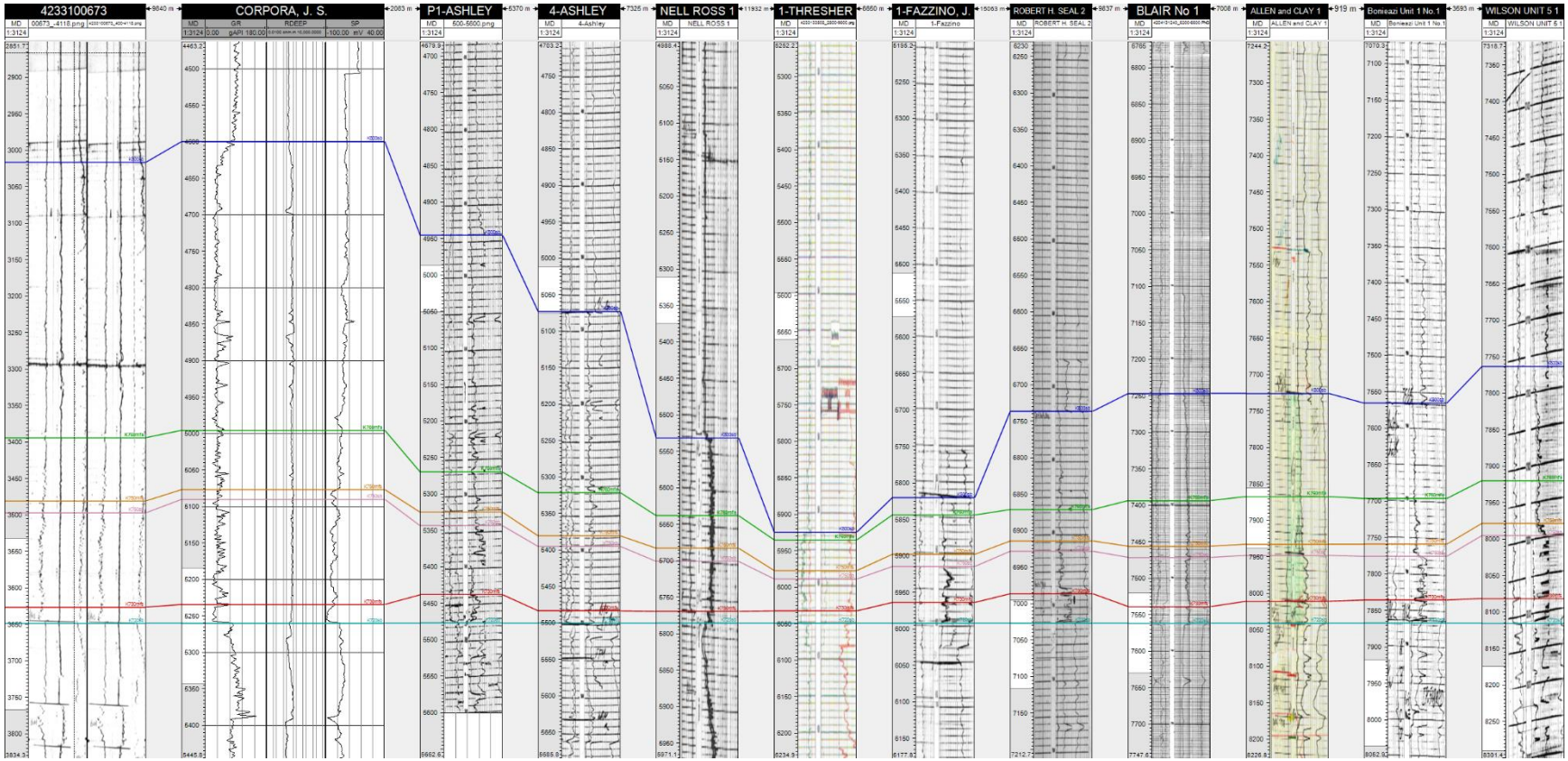

Figure A4. Cross section E-W: #4. West to East oriented cross section of the Austin Group with internal sequence boundaries and maximum flooding surfaces .

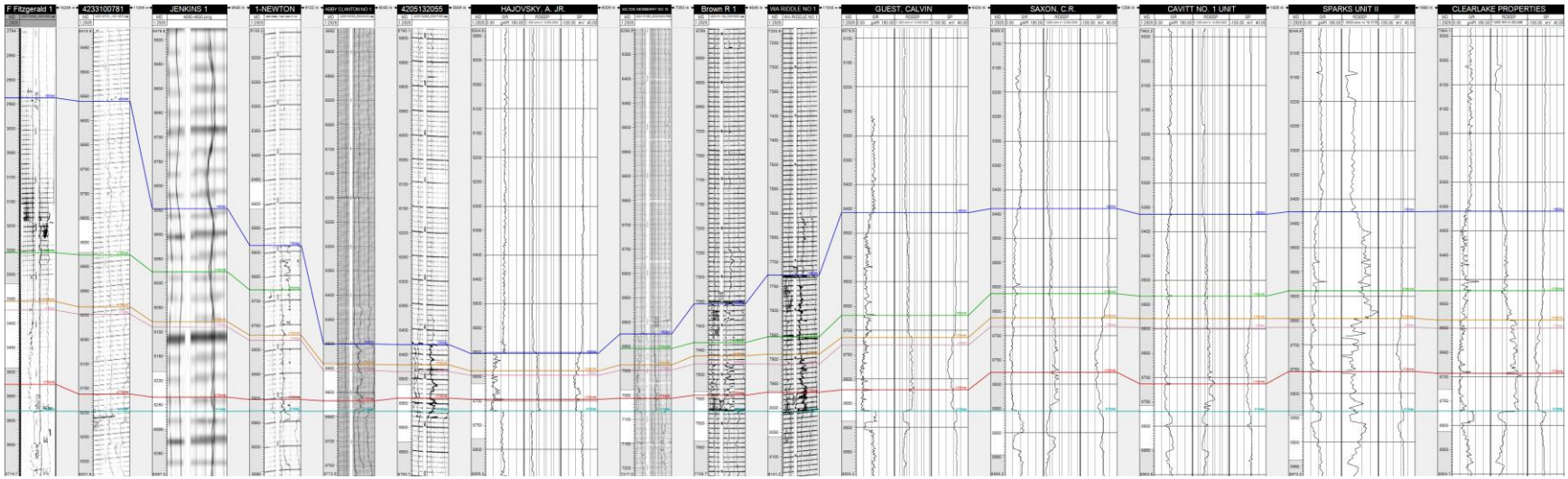

Figure A5. Cross section E-W: #5. West to East oriented cross section of the Austin Group with internal sequence boundaries and maximum flooding surfaces .

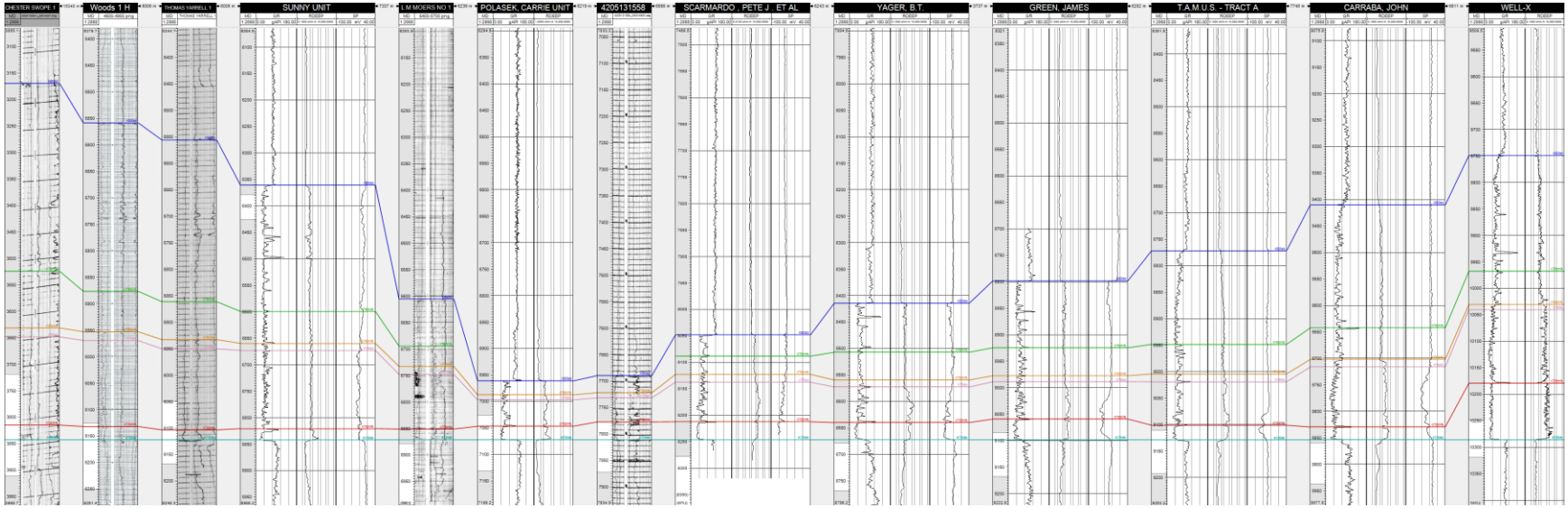

Figure A6. Cross section E-W: #6. West to East oriented cross section of the Austin Group with internal sequence boundaries and maximum flooding surfaces .

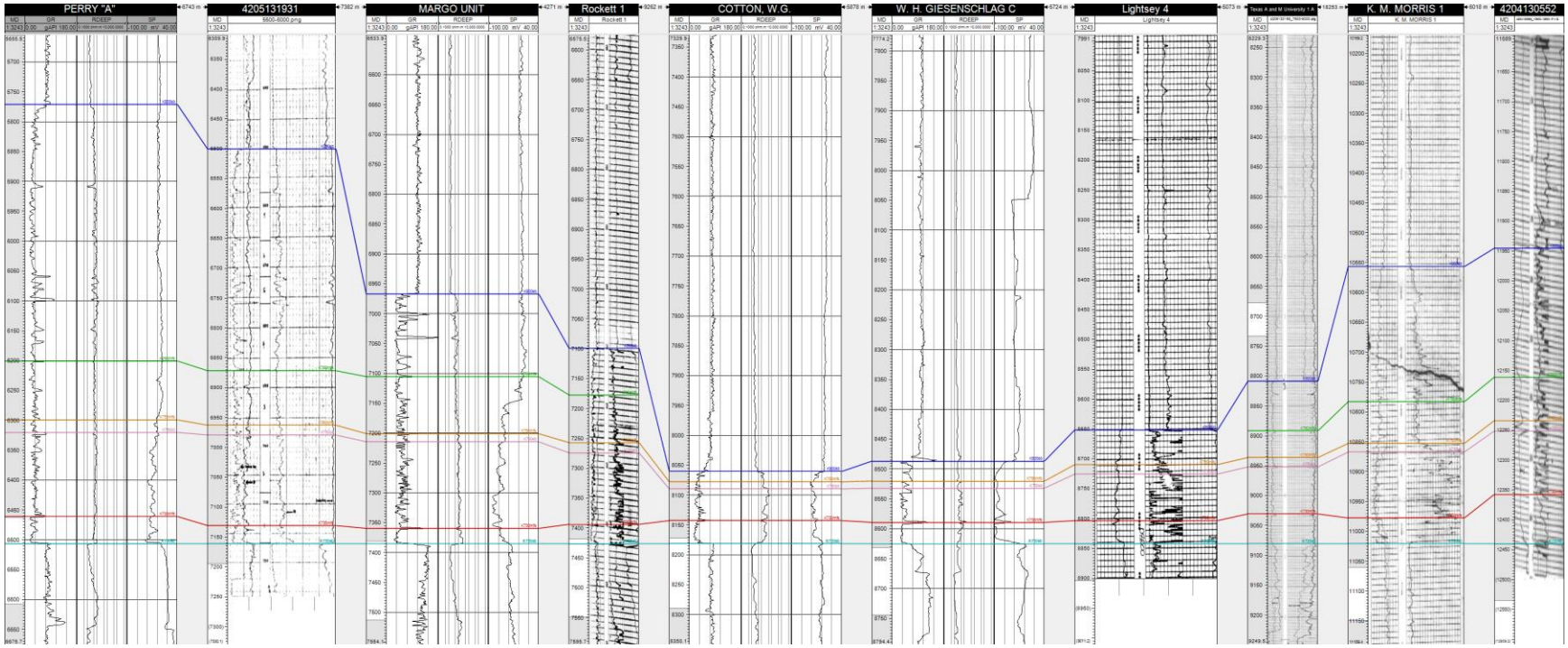

Figure A7. Cross section E-W: #7. West to East oriented cross section of the Austin Group with internal sequence boundaries and maximum flooding surfaces .

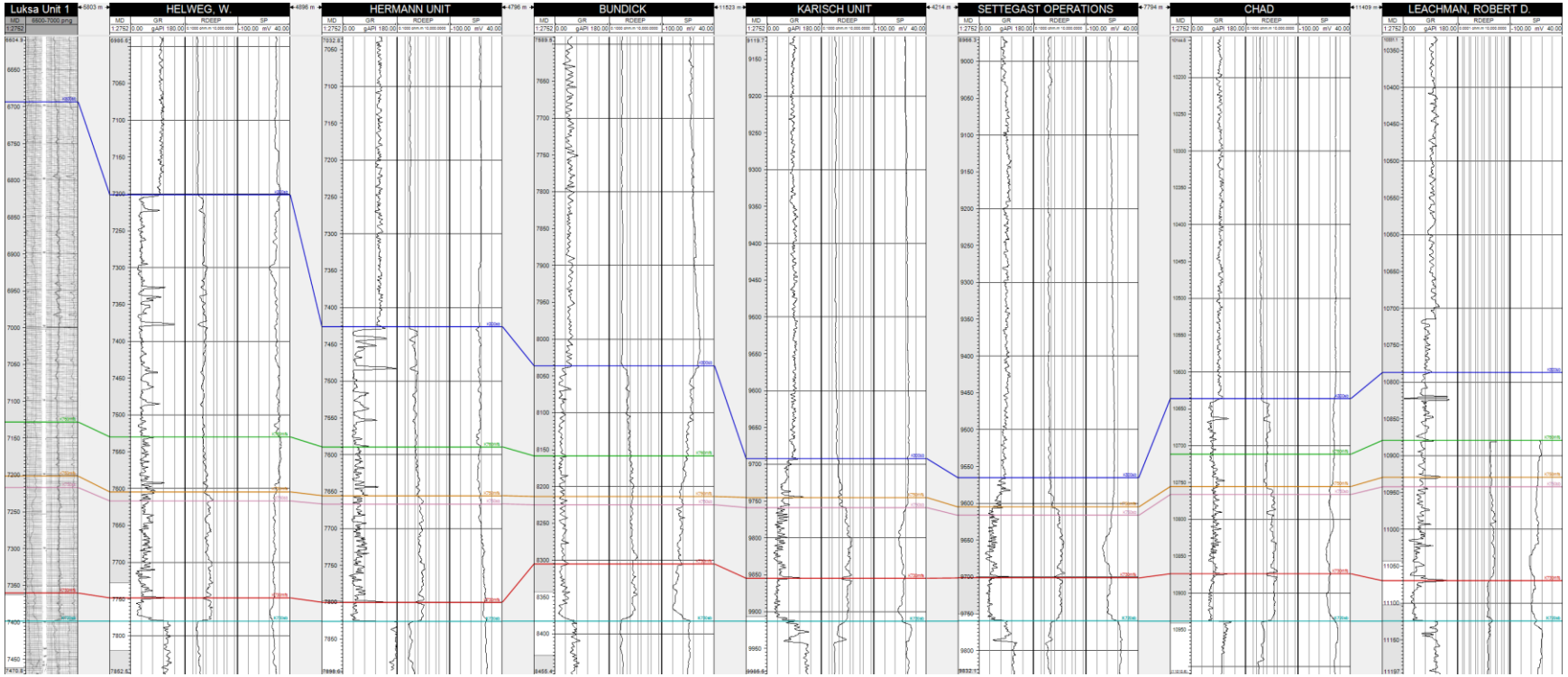

Figure A8. Cross section E-W: #8. West to East oriented cross section of the Austin Group with internal sequence boundaries and maximum flooding surfaces .

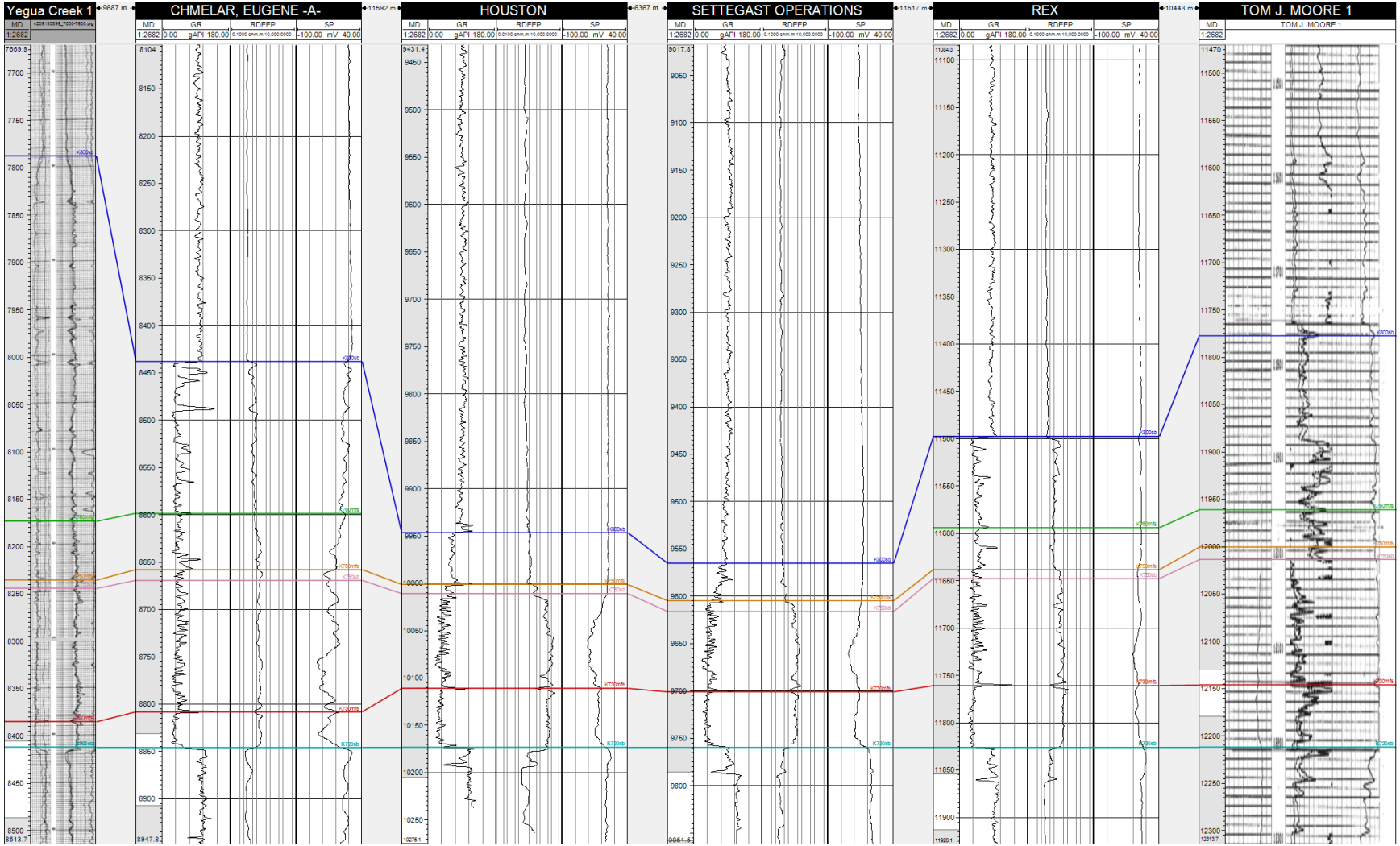

Figure A9. Cross section E-W: #9. West to East oriented cross section of the Austin Group with internal sequence boundaries and maximum flooding surfaces .

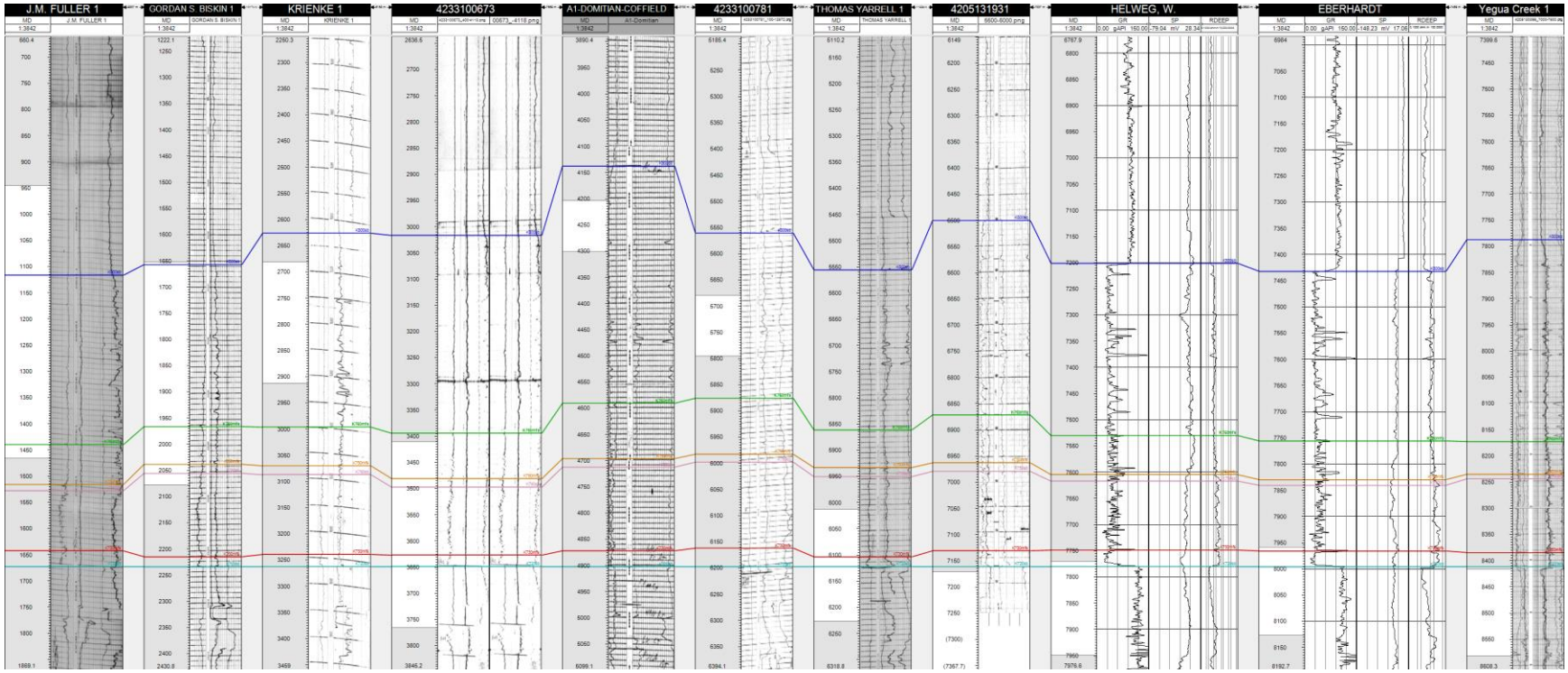

Figure A10. Cross section N-S: #1. North to South oriented cross section of the Austin Group with internal sequence boundaries and maximum flooding surfaces .

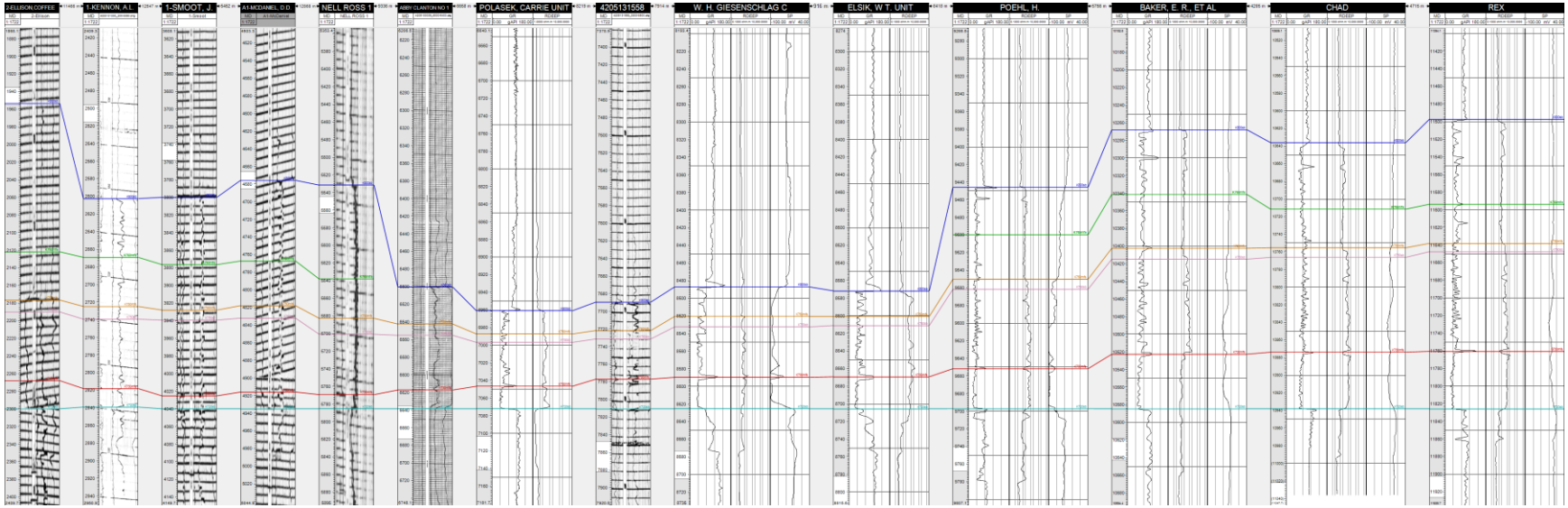

Figure A11. Cross section N-S: #2. North to South oriented cross section of the Austin Group with internal sequence boundaries and maximum flooding surfaces .

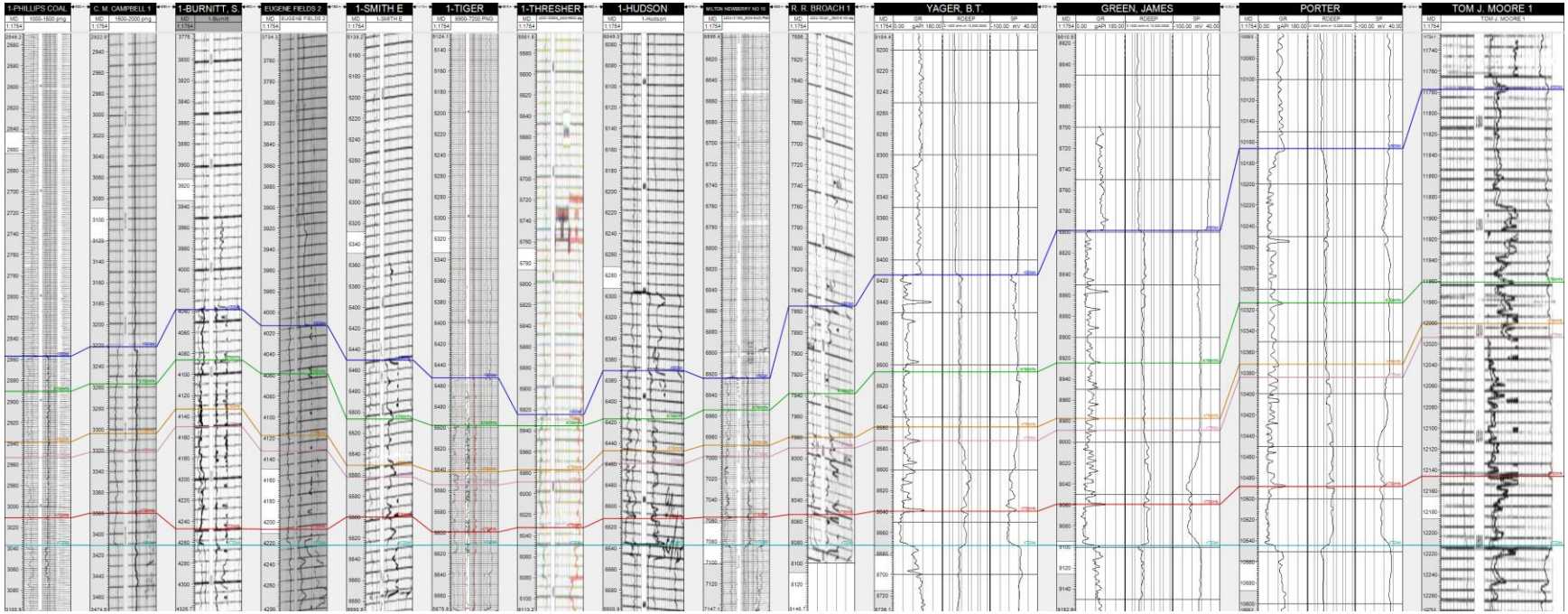

Figure A12. Cross section N-S: #3. North to South oriented cross section of the Austin Group with internal sequence boundaries and maximum flooding surfaces .

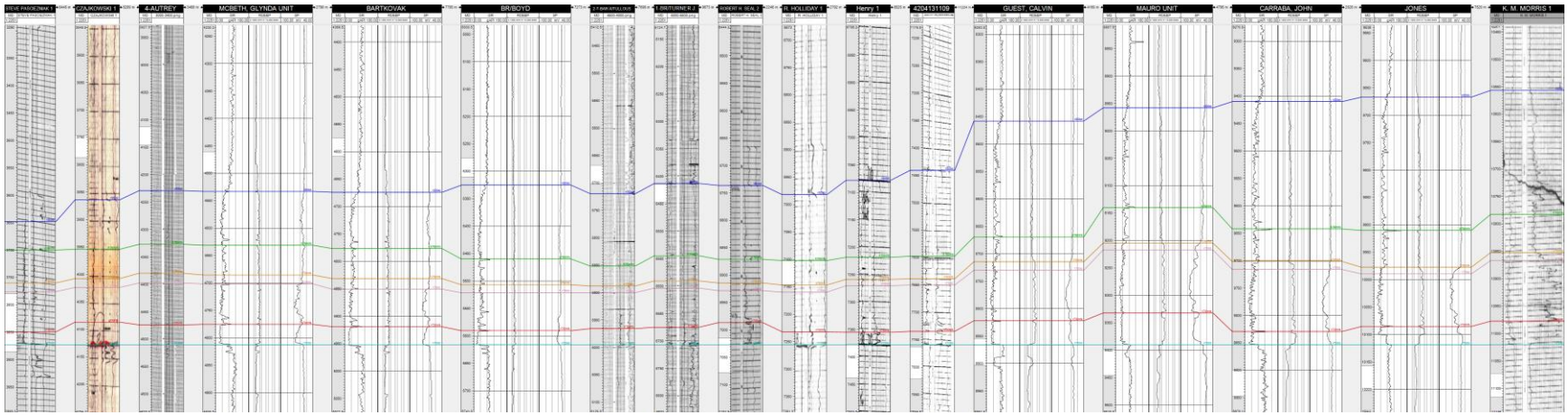

Figure A13. Cross section N-S: #4. North to South oriented cross section of the Austin Group with internal sequence boundaries and maximum flooding surfaces .

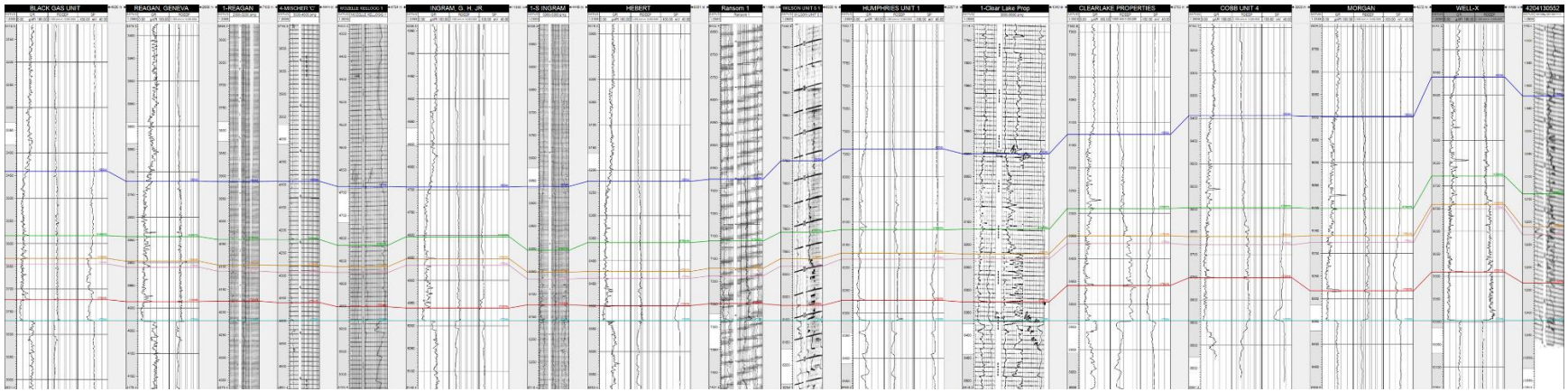

Figure A14. Cross section N-S: #5. North to South oriented cross section of the Austin Group with internal sequence boundaries and maximum flooding surfaces .

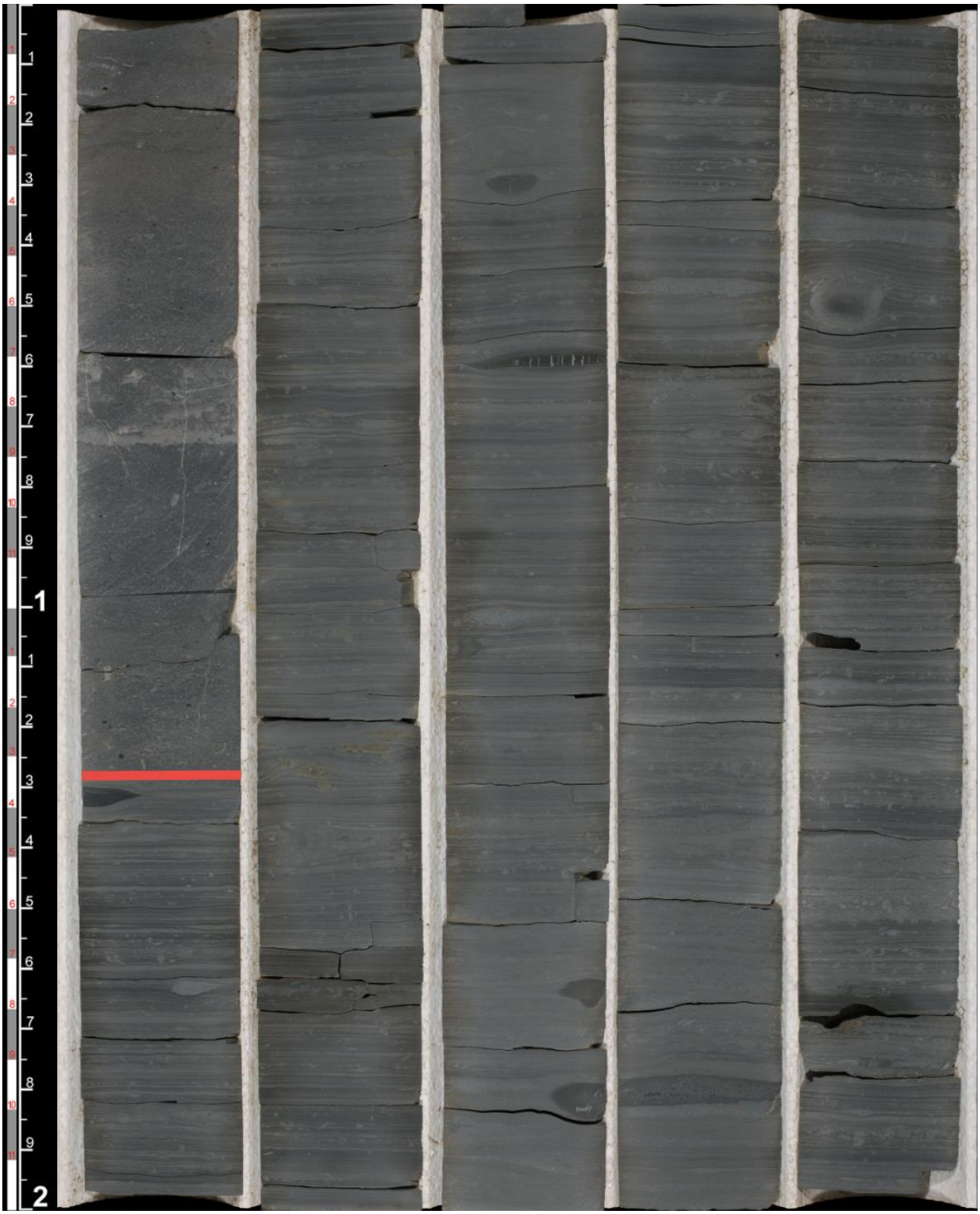

Figure A15. Core photo of the Eagle Ford and Base Austin boundary (K720sb). Boundary marked in red.

Figure A16. Core photo of the Upper and Lower Austin boundary (K750sb). Boundary marked in red.